Original Investigation

A Review of Radiomics and Deep Predictive Modeling in Glioma Characterization

Sonal Gore, M.Tech, Tanay Chougule, BE, Jayant Jagtap, PhD, Jitender Saini, MD,DM, Madhura Ingalhalikar, PhD

Recent developments in glioma categorization based on biological genotypes and application of computational machine learning or deep learning based predictive models using multi-modal MRI biomarkers to assess these genotypes provides potential assurance for optimal and personalized treatment plans and efficacy. Artificial intelligence based quantified assessment of glioma using MRI derived handcrafted or auto-extracted features have become crucial as genomic alterations can be associated with MRI based phenotypes. This survey integrates all the recent work carried out in state-of-the-art radiomics, and Artificial Intelligence based learning solutions related to molecular diagnosis, prognosis, and treatment monitoring with the aim to create a structured resource on radiogenomic analysis of glioma. Challenges such as inter-scanner variability, requirement of benchmark datasets, prospective validations for clinical applicability are discussed with further scope for designing optimal solutions for glioma stratification with immediate recommendations for further diagnostic decisions and personalized treatment plans for glioma patients.

Key Words: Glioma; Biomarkers; Machine Learning; Deep Learning; Radiogenomics; Radiomics.

INTRODUCTION

Gliomas are one of the most life threatening and commonly occurring brain neoplasms with an average age adjusted annual incidence of 6 to 10 per 100,000 population depending upon the geographical region (1–3). These tumors originate from the glial cells and have an ability to rapidly infiltrate the surrounding healthy tissues making it one of most disparaging malignant tumors. Early diagnosis and timely management of these tumors is crucial as glioma pathogenesis is highly complicated with rapid infiltration of the surrounding parenchyma and despite intensive multimodal management involving surgical resection, adjuvant radiotherapy, and chemotherapy with temozolomide, outcomes are often poor (4).

Acad Radiol 2020; ■:1–23

From the Department of Electronics and Telecommunications, Symbiosis Institute of Technology, Symbiosis International University, Pune India (S.G., J.J.); Department of Radiology, National Institute of Mental Health and Neurosciences, Bengaluru, India (J.S.); Symbiosis Center for Medical Image Analysis, Symbiosis International University, Pune, India (T.C., M.I.). Received May 12, 2020; revised June 11, 2020; accepted June 11, 2020. **Address Correspondence to:** M.I. e-mail: head@scmia.edu.in

https://doi.org/10.1016/j.acra.2020.06.016

Glioma Classification

The classification of brain tumors is broadly based on the histological resemblance of tumor cells with their possible cells of origin. These histological similarities are usually determined based on the microscopic features in hematoxylin and eosin-stained sections, immunohistochemistry, and ultrastructural features (5). Based on the histopathological characteristics the tumors are classified into Grade I to Grade IV lesions. Low grade gliomas (LGGs) include oligodendroglioma and astrocytoma while grade III gliomas are anaplastic oligodendroglioma and astrocytoma. Grade IV also known as glioblastoma and gliosarcoma are the most commonly occurring and highly infiltrative tumors (6). Glioblastoma have a very low survival period of approximately 15 months with the strongest prognostic factors being age and extent of resection (7).

New emerging knowledge over the period of last twenty years clearly demonstrates that specific genetic alterations are significantly linked with tumorigenesis and characterize certain common and rare tumor entities (8). Growing body of evidence suggests that molecular genotypes in addition to histopathology significantly impacts the survival of the patient (9,10). Such categorization of gliomas is therefore critical as it improves prognostication with potential to support patient-specific treatment plans and tailored therapeutic interventions. This compelling information was quickly incorporated in the revised brain tumor classification in the year 2016 by

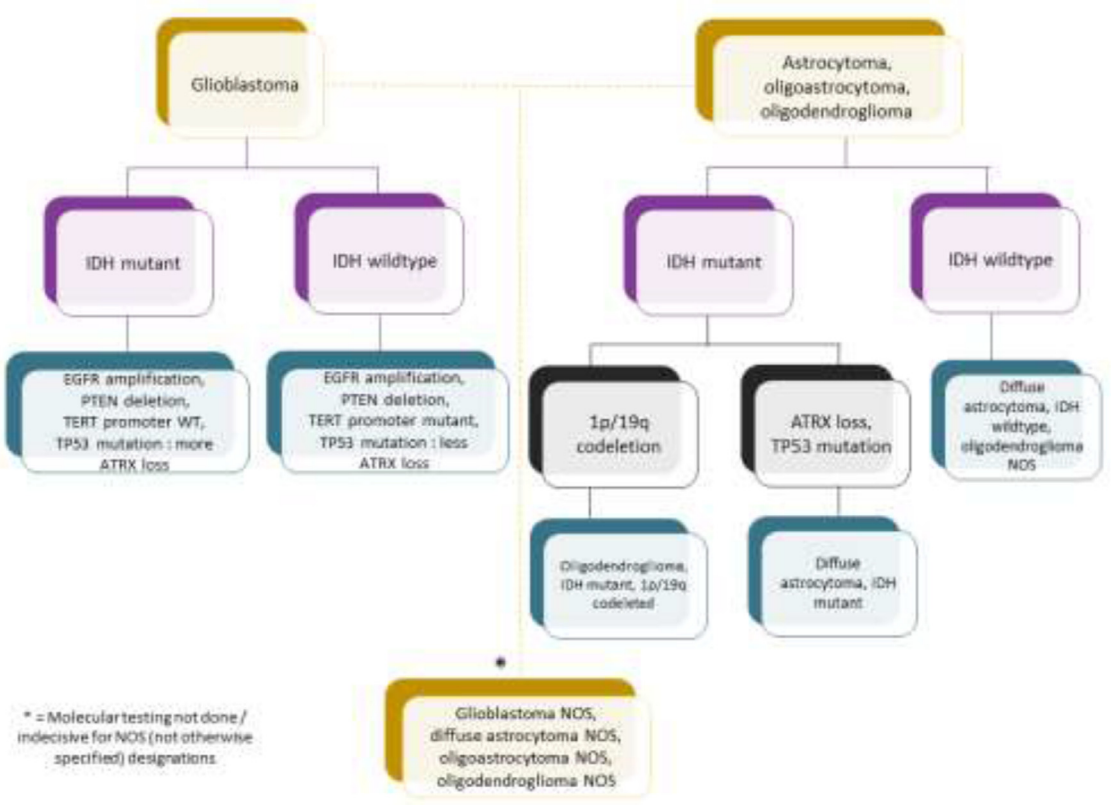

Figure 1. The overall classification of glioma as per WHO 2016 edition. The above hierarchical structure shows the classification with histological subtypes of glioma at first layer, followed by associated genotypes with integrated diagnosis at next layers. Abbreviations: IDH, isocitrate dehydrogenase; WT, wild type; EGFR, epidermal growth factor receptor; PTEN, phosphatase and tensin homolog; TERT, telomerase reverse transcriptase; TP53, tumor suppressor protein p53; ATRX, alpha thalassemia/mental retardation syndrome X-linked; NOS, not otherwise specified.

the World Health Organization (WHO) where for the first time histological and genetic information (genotype and phenotype) was used together for classifying as well as characterizing brain tumors (11).

Currently, one of the key known factors in predicting survival is the presence or absence of the isocitrate dehydrogenase (IDH) (IDH 1 and IDH 2) genotype (12–14). IDH 1 and 2 are metabolic enzymes converting isocitrate to α-ketoglutarate (αKG) and confer neomorphic activity in the mutant protein, resulting in the conversion of αKG to the oncometabolite, D-2-hydroxyglutarate (15–17). The subsequent accumulation of D-2-hydroxyglutarate results in epigenetic dysregulation via inhibition of αKG-dependent histone and DNA demethylases, and may block cellular differentiation (18). The mutation can be identified even in the early process of oncogenesis in low as well as high grade gliomas and is often associated with increased methylation in glioma (19). Based on this mutation, glioma subtypes are now being considered either as IDH positive (mutant) or IDH negative (wildtype) (11,15,20). Another important genetic alteration associated with low grade gliomas is the presence or absence of 1p/19q codeletion, which refers to the loss of short arm of chromosome 1(1p) and the long arm of chromosome 19 (19q). IDH mutant types of grade II and III can be further sub-classified based on the presence or absence of 1p/19q co-deletion (21–23). All 1p/19q co-deleted gliomas are IDH1 mutated at arginine 132 or the analogous residue arginine 172 in IDH2 and are classified as oligodendroglioma (11). Other genetic alterations include mutations in telomerase reverse transcriptase (TERT) gene promoter (24,25), methylation of the methyl-guanine methyl transferase (MGMT) gene promoter (26), epidermal growth factor receptor variant III (EGFRvIII) (27), alpha thalassemia/mental retardation syndrome X-linked (ATRX) loss (28), tumor suppressor protein p53 (TP53), and phosphatase and tensin homolog mutations etc. (29). The overall classification as per WHO 2016 edition is presented in Figure 1 with subtypes, genotypes and grade.

Other than these techniques, glioma heterogeneity can also be characterized using transcriptomic profiling identifying the tumors as proneural, mesenchymal, classical, and neural (27). Furthermore, epigenetic phenotypes may also provide critical insights into the intertumoral classification and natural history (30).

Currently, histopathology followed by immunohistochemistry and Deoxyribo-Nucleic Acid (DNA) sequencing is required after biopsy or complete resection of the tumor and is essential for correct subtyping of the tumor.

In case this facility is not available, tumor is labeled as per its histopathology followed by not otherwise specified (8,11,31,32). These tests are considered as gold standard and have shown to facilitate accurate diagnosis by correctly identifying both histopathological subtype as well as the mutation status.

One of the critical factors for poor response to therapy and rapid recurrence is intra tumoral heterogeneity (33) where the variation may occur structurally within a tumor with substantial sub-clonality that may include a composite of molecularly distinct tumoral areas with no uniformity. Gaining deeper understanding of intra-patient tumoral heterogeneity is therefore crucial. Previous studies using molecular biology, histo-pathology techniques have tried to characterize intra-tumoral heterogeneity, however, exhibit several limitations. These tests are highly dependent on the tissue samples obtained and are therefore restricted to a specific spatial location within the heterogeneous tumor. In cases where part of tumor is left behind due to widespread lesion or because of involvement of eloquent cortex as well as in cases with multifocal lesions the lesion will be classified based on the sampled tissue that may fail to provide a comprehensive marker as the left behind tumor may be pathologically different. Furthermore, an invasive resection to sample for spatial context may add to the risk of significant morbidity when lesion is present in an eloquent location (34). Finally, the complexity of coverage of the assay may impose challenges in multi-institutional clinical comparisons (35).

Emerging work has started focusing on quantitative markers of genotype information that can be captured from the first magnetic resonance imaging (MRI) scan as it would not only provide a noninvasive preoperative prognosis of the grade/mutational status but will also enable patient specific treatment plan early on and support therapeutic intervention. Especially, quantitative methods such as use of image textures and intensity features which are broadly termed as 'radiomics' play a vital role in creation of prognostic markers for gliomas (36). Usually, these multiple features are expected to facilitate complementary information and consequently are used in a multivariate machine learning framework to create a distinct probabilistic biomarker. Moreover, recent advances in artificial intelligence (AI) such as deep learning (DL) have become critical in computer aided diagnostic (CAD) methods and have been applied to predict the genomic properties of tumors from radiological images (37). The utilization of image features and data informatics to predict tumor genotypes has been largely termed as 'radiogenomics', and is a forthcoming area of interest with enormous amount of research carried out in the recent few years (38,39).

MR Imaging in Gliomas

MRI is an advanced medical imaging technique and is generally used as a primary care in tumor patients to identify the neoplasm. The MR images facilitate a detailed image of soft tissues at a high resolution and in multiple contrasts. In case of neuro-malignancies clinics generally acquire either a 2D or 3D MRI scan depending on the site, expenditure, time required for acquisition and clinical/research interests (40). MRI sequences that are commonly acquired for tumor cases include T1-weighted MRI, T1-weighted MRI with contrast enhancement (T1-CE), T2-weighted MRI, and T2-weighted with Fluid Attenuated Inversion Recovery (T2-FLAIR). Advanced MRI techniques including diffusion weighted imaging (DWI) to compute apparent diffusion coefficient maps (ADC), diffusion tensor imaging (DTI) to measure mean, radial and axial diffusivity and/or fractional anisotropy, functional resting state MRI using the blood oxygen level dependent contrast, perfusion weighted imaging (either dynamic susceptibility contrast (DSC) or dynamic contrast enhanced (DCE)) to compute the cerebral blood flow (CBF) and cerebral blood volume (CBV), amide proton transfer (APT) imaging to reflect the cellular proliferation in tissues and magnetic resonance spectroscopy (MRS) may also be acquired.

Diffusion MRI can be acquired using multiple shells for example at b = 500, 1000, 2000 s/mm$^{\wedge 2}$ as it enables computing multicompartment which extracts the extra-cellular free water (FW) that may support in delineating vasogenic edema from infiltration (41). Standard models such as bi-tensor model (42) or neurite orientation and dispersion density imaging (NODDI) (43) can be employed to extract the free water. Perfusion scans of DSC and DCE require gadolinium-based contrast agent, where DSC parameters are computed from the first pass of the contrast agent (bolus tracking) while for DCE exploits T1-shortening effects of gadolinium (44−46). Arterial spin labeling is another technique that does not require any contrast to compute the gain CBF, albeit provides low signal to noise ratio (47). The choice of perfusion imaging depends on the clinician and the team's interest, however majority centers rely on DSC or DCE imaging. APT, a recent modality is typically acquired only with research interests as it has illustrated promising results in brain tumors (48). It involves magnetization transfer (MT) imaging where the signal loss in tissues with high protein content and water- macromolecule interactions in captured (49). Figure 2 shows a sample MRI acquisition in clinical neuro-oncology.

Identification of the tumor genotypes from visual inspection is highly complicated and is practically unattainable in standard radiology practice. However, these modalities, together for a large patient population, can be used in a multivariate framework that usually involves the use of machine learning algorithms, not only to learn the underlying patterns of features from numerous subjects but also to provide a meaningful probabilistic marker for the subtype, genotype or grade. In addition, the learned model can be used to test new cases effortlessly and can be applied in radiology workflow to plan patient-specific treatment and management.

Radiomics

Radiomics is an emerging translational field where an array of attributes that include geometry, intensity and histogram features as well as image textures are computed from radiographic images to capture the phenotypic patterns and may illustrate a distinguishing marker for glioma subtypes. The

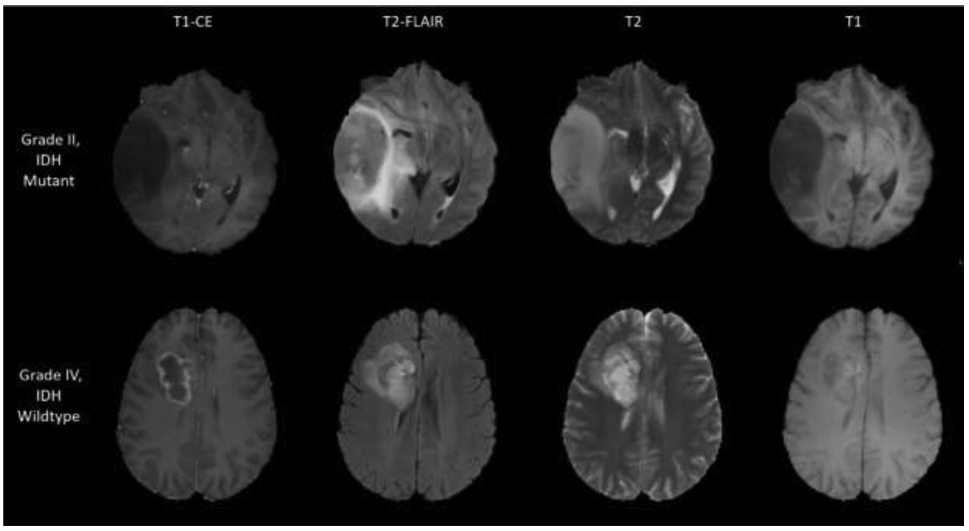

Figure 2. Sample MRI acquisition in neuro-oncology. Figure shows eight axial slices of two patients from the TCIA dataset. In the top row, brain MRI images from a 28-year-old male with Oligoastrocytoma (Grade II, IDH Mutant), whereas in the bottom row, images from a 33-year-old female with Glioblastoma (Grade-IV, IDH-Wildtype) are shown. From left to right: two slices are of each modality namely T1 contrast enhanced (T1-CE), T2-weighted with Fluid Attenuated Inversion Recovery (T2-FLAIR), T2-weighted, T1-weighted are shown.

features include shape features such as volume, sphericity, mesh surface area etc., histogram features that may include mean, median, energy, entropy, 10 percentile intensity, 90 percentile intensity etc., and texture features of Gray-Level Co-occurrence Matrix, Gray-Level Dependence Matrix, Gray-level Run Length Matrix, Gray Level Size Zone Matrix and Neighboring Gray Tone Difference Matrix etc. A detailed list of standard features can be found in (50). Usually, radiomics is used in multi-variate predictive framework for the purposes of prognosis, disease tracking and evaluation of response to treatment (51). In neuro-oncology, radiomics is gaining momentum for non-invasive prediction of the type of neoplasm, tumor grading as well as genomic and transcriptomic subtyping (52). Typically, analysis with MR based radiomics in neuro-oncology includes the following steps: (1) data acquisition, (2) brain extraction and data cleaning/denoising, (3) intensity normalization (4) inter-modality registration (5) tumor segmentation (manual or semi-automated)

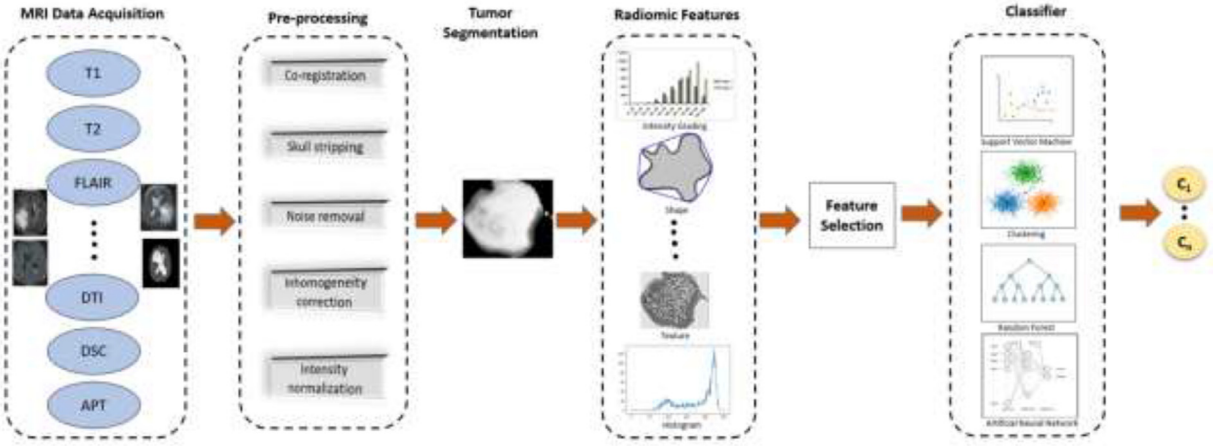

Figure 3. Typical flow of multimodal radiomic based predictive approach for glioma classification. It is a block diagram outlining the usual functional steps to carry radiomic analysis of brain tumor. Any generic radiomic process follows few or all above steps to predict tumor genotypes. The steps like MRI preprocessing, feature selection may be performed in such workflow execution. MRI data acquisition includes the scans taken from conventional as well as advanced modalities including T1-weighted, T2-weighted, T2-weighted with Fluid Attenuated Inversion Recovery (FLAIR), diffusion tensor imaging (DTI), dynamic susceptibility contrast (DSC), amide proton transfer (APT), etc. Preprocessing involves different tasks such as co-registration, skull stripping, noise removal, bias correction, intensity normalization, inhomogeneity correction, slicing, etc. The region of interest (ROI) can be segmented manually or using automatic or semi-automatic method. Further step focuses on extraction of various semantic features like tumor size, location etc. as well as computational features including texture, shape, statistical, histogram, intensity etc. The most discriminant features may be selected and further used for classification into 'n' number of classes using different machine learning classifiers including support vector machine, random forest, K nearest neighbor, k-means, adaboost, decision tree, artificial neural network, etc.

(6) feature extraction (Radiomics), (7) feature selection, and (8) multivariate classification, followed by cross-validation and testing (53). The most discriminative features are usually highlighted as these may facilitate clinical interpretability. Figure 3 shows the typical flow for classification using radiomics on multi-modal MRI in neuro-oncology.

Deep Learning

Recent discoveries in Artificial Intelligence have illustrated exceptional performance in complicated tasks by allowing machines to better characterize and interpret the underlying complex information. Non-deterministic deep learning models are loosely inspired by how the human brain works during learning and/or execution of a task, and these facilitate more automated and precise performance (54). Convolutional neural networks (CNNs), a type of deep learning architecture where convolutions on the image capture the features that are optimized to learn the task at hand, have proven to be especially useful in medical image analysis (55). These have the capability to automatically extract image attributes (features) in hierarchical manner from local to global representation of images effectively finding important features as part of its search process and eliminating the steps of manual feature engineering and selection that are required in machine learning. Figure 4 shows the typical CNN architecture and its workflow. Recent growing evidence demonstrates superior performance of CNN for genotype prediction such IDH mutation and has been discussed in the following pertinent sections.

This paper aims at comprehensively reviewing studies that have proposed and utilized MRI based techniques for prognostic molecular subtyping of gliomas using radiomics and/or AI based methods. The paper also discusses the current challenges in clinical translation and future scope of such techniques.

METHODS

Our current review is focused on gliomas and particularly on the molecular subtype delineation and grading based on multi-modal MRI. Most of the studies have explored the idea of association of imaging features with specific genotypes either using basic intensity, volume-based attributes or by

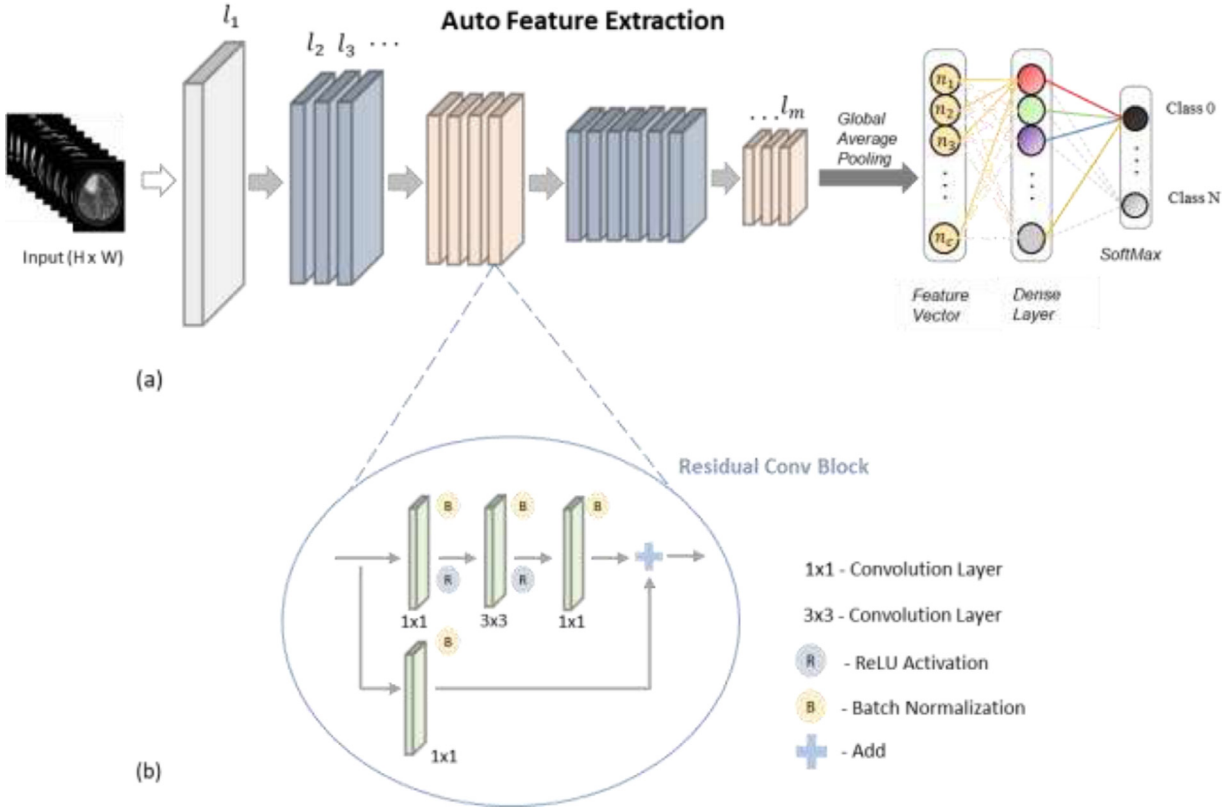

Figure 4. Typical CNN architecture for glioma classification. (a) represents ResNet50 – a frequently used convolutional neural network (CNN) model for glioma genotyping. A CNN model consists of *'m'* convolutional blocks ($l_1, l_2 \ldots, l_m$), typically followed by a global average pooling. A feature vector of size *'c'* is obtained after global average pooling of the output of the final convolutional block (l_m) with *'c'* convolutional layers. The feature vector is fed to fully connected dense layer(s) and finally to a SoftMax layer to obtain output class probabilities. (b) represents a residual convolutional block used in ResNet architectures. The residual blocks consist of two *'1 × 1'* and one *'3 × 3'* convolutional layers followed by batch normalization and activation layers. The residual blocks leverage residual connections (skip connection) to stack large number of layers in CNN architectures.

employing more complex models of radiomics with multivariate learning and DL. We extensively searched the PubMed database with combinations of keywords "glioma molecular classification", "IDH", "MGMT", "1p/19q", "EGFR", "Glioblastoma" "radiogenomics", "radiomics", "machine learning", "support vector machine", "random forest", "convolutional neural nets", "residual nets" and "deep learning", "glioma survival prediction", "MRI", "WHO grading", "low grade glioma", "high grade glioma", and "classification" to gather the published work using multimodal MRI based features for predicting the grade and on characterizing genetic profiles that include IDH, 1p/19q codeletion, EGFR variant III (EGFRvIII), methylation status of MGMT, other genetic profiles (TERT, TP53, phosphatase and tensin homolog etc.) and transcriptomic compositions of Glioblastoma (classical, mesenchymal, proneural, and neural), grading, and survival prediction. Table 1 and 2 summarize the state of art research focusing on radiogenomics where radiomics/machine learning (Table 1) or DL based (Table 2) algorithms have been employed to predict the molecular subtypes.

Radiomics and deep learning methods have been commonly used to assess the tumor grade as well as to predict survival in glioblastoma patients. Table 3 summarizes the multivariate predictive studies performed to assess the tumor grade and survival.

RESULTS AND DISCUSSION

IDH

IDH1 mutations are more frequent in younger patients with grade II gliomas or secondary glioblastoma, and are generally found to have more encouraging outcomes of higher survival (16). Multiple studies have focused on the problem of delineating IDH mutant gliomas from IDH wildtype from multimodal MR images and associating the radiophenotypic characteristics to the mutation. Multiple studies on large and small group of subjects (ranging from 25−750 subjects) using a myriad of computational predictive models on multi-modal MRI have demonstrated that IDH mutation can be identified with very high accuracies ranging from 85% to 97% (56,57).

Earlier techniques relied on single (T2-weighted MRI or FLAIR or DTI) or fewer (two to three) modalities and exemplified gross features such as tumor volume (58), location of the neoplasm (59,60), enhancement on T1-CE, larger proportion of non-enhancing tumor and extent of FLAIR hyper-intensity (61) to potentially correlate with IDH mutation and can be considered as gross visual features to identify the mutation (62,63). Another key feature that has been studied extensively is the T2-FLAIR mismatch sign among non-enhancing low-grade gliomas. The mismatch sign (as shown in Figure 2) displays relatively hypo-intense signal on FLAIR throughout the majority of the lesion compared to T2-weighted with the exception of the peripheral rim of hyper-intense signal and is indicative of IDH-mutant, 1p/19q non-codeleted astrocytoma (64,65). Although the sign is highly specific in identifying IDH-mutant, 1p/19q non-codeleted astrocytoma, the mismatch intensities vary significantly with the scanning protocol consequently facilitating lower inter-rater agreement and inferior sensitivity (sensitivity = 10.9%, specificity = 100%) (66). Moreover, the cause for mismatch sign is unclear and biological elucidation is necessary (65).

In terms of other advanced modalities, perfusion weighted imaging has demonstrated higher relative CBV (rCBV) in IDH wildtype cases while diffusion MRI based studies have illustrated lower ADC values in IDH mutant cases (67,68). However, all the above discussed features are not sensitive to the variability that has been observed between patients making it complicated to assign a precise and robust biomarker.

Instead of relying on a single feature of interest, extraction of multiple imaging features such as image textures, intensity features etc., and pooling these into a multivariate framework may provide more sensitivity and predictive power. To this end, radiomics with predictive models have been employed to identify IDH mutation. The majority of the studies to this date have mainly focused on the online open-source TCIA (The Cancer Imaging Archive) data (56,69−73) while remaining studies have employed local datasets (74−80) (as listed in Table 1). Studies on TCIA have demonstrated IDH predictive accuracies ranging from 72-95% while on other datasets the accuracies ranged from 73-90% based on multimodality features (T1, T1-CE, FLAIR, and T2). A consensus from all these studies shows that the attributes computed from T1-CE and FLAIR have been highly distinctive of IDH mutation than the ones computed from T1 and T2 weighted MRI. In addition to these, work on diffusion imaging has been promising where radiomics on fractional anisotropy (FA) and diffusion kurtosis can be crucial in delineating IDH genotype (81,82). Lower mean diffusion kurtosis measures with area under curve (AUC) of 0.88 and local binary patterns (LBP) on FA (with AUC of 0.92) have been highly discriminative of the IDH mutation (83). At the same time, however, advanced diffusion models such as NODDI may not play any significant role in the classification with a non-significant p-value in the range of 0.3 to 0.9 (82). Nonetheless the utility of multi-compartment models using multi-shell diffusion acquistion has not yet been extensively evaluated.

The features of importance have been highly dependent on the grade of the tumor under consideration. For example, Javier et al. reported that ADC feature maps were more discriminative in grade II gliomas where IDH wildtype were highly associated with lower ADC values with poor clinical outcomes (61), however a similar trend was not observed in high grade gliomas (84). Similar findings were also illustrated by Matteo-Figini et al. (82). Recent work has started focusing on textural analysis on advanced modalities such as DSC images and has illustrated that DSC features alone can predict IDH mutation with an accuracy of 71% (85).

Other than radiomics, deep neural nets have been widely used to delineate gliomas with IDH mutation. Specifically, CNNs

TABLE 1. Summary on Experimentation and Results of Research Work Using Radiomic Methods. It Summarizes the State-of-art Research Focusing on Radiogenomics Where Multimodal Radiomic Analysis Using Machine Learning Based Algorithms Have Been Employed to Predict the Molecular Subtypes of Glioma. It Provides the Summary Details for Histological Subtypes Used, Genotypes, Number of Classes Used, Number of Patients, MRI Modalities Used, Dataset Used, Number of Features Extracted, List of Features, Machine Learning Method (ML), Evaluation Method, and Performance Measures. Multivariate Analysis is Assessed Using Train-Test Split Method, 5-Fold or 10-Fold Cross Validation Method. Evaluation is Performed on Freely Online Available and/or Local Datasets. Performance Measures Used are Accuracy, Area Under Curve (AUC) Value, *p*-Value, Sensitivity, Positive Predictive Value (PPV), Negative Predictive Value (NPV), and Sensitivity

Reference Details, Year	Glioma histological Subtype	[Glioma genotype], [No. of classes]	[Sample size], [MRI modality], [dataset]	[No. of features], [Feature list]	[ML method], [Evaluation method]	Performance Testing
Wu (56), 2019	LGG, HGG	[IDH mutant, IDH wild], [2]	[126], [T1, T1-CE, T2, T2-FLAIR], [TCIA]	[704], [GLCM texture, Volume, intensity, histogram, diffusion]	[SVM, KNN, RF, NB, ANN, FDA, Adaboost], [10-fold cross validation]	Accuracy: 88.5 % for RF algorithm
Qi (59), 2014	LGG, HGG (Astrocytoma)	[IDH1/2 mutant, IDH wild], [2]	[193], [Local]	[intensity, growth pattern-location, tumor margin, contrast enhancement, mass-edema effect]	[2-sided Chi-square statistical test]	p-value: $<$0.001 for IDH wild in combined lobes, p-value: $<$0.001 for IDH mutant in less-risk regions
Villanueva-Meyer (61), 2018	LGG (Grade II)	[IDH mutant, IDH wild], [2]	[100], [T1, T2, T2-FLAIR, DWI, DSC, SPGR],	[Location, extent, margin sharpness, cystic component, contrast, diffusion& perfusion measures]	[Logistic regression]	ADC_{min} sensitivity: 91%
Ding (62), 2019	LGG	[IDH mutant, IDH wild], [2]	[76], [T1, T2, T1-CE, FLAIR]	[Location, tumor border, cystic change, presence of edema, contrast enhancement, MRS (choline/creatine ratio)]	[Logistic regression]	Accuracy: 79.3 % with MRS parameter, p-value: Cortical involvement-0.0001, edema-0.0381, border-0.0287
Wang (63), 2019	HGG (Glioblastoma)	[IDH1 mutant, IDH1 wild], [2]	[50], [T1, T2, T1-CE, FLAIR]	[age, location, volume, contrast enhancement]	[Logistic regression]	AUC: 0.88
Broen (65), 2018	LGG	[diffuse astrocytoma IDH mutant 1p/19q non-codeleted, diffuse oligo-dendroglioma IDH mutant 1p/19q co-deleted, anaplastic astrocytoma IDH mutant 1p/19q non-codeleted, anaplastic oligodendroglioma IDH mutant 1p/19q co-deleted, diffuse astrocytoma IDH wild], [5]	[154], [T2 FLAIR]	[T2 FLAIR mismatch sign, location, sex, age, grade]	[statistical analysis]	PPV: 100%, NPV: 68%

(*continued on next page*)

TABLE 1. (Continued)

Reference Details, Year	Glioma histological Subtype	[Glioma genotype], [No. of classes]	[Sample size], [MRI modality], [dataset]	[No. of features], [Feature list]	[ML method], [Evaluation method]	Performance Testing
Jagtap (69), 2019	LGG, HGG	[IDH mutant with 1p/19q co-deletion, without co-deletion], [2]	[T2]	[LBPH texture, statistical, histogram, intensity grading]	[ANN], [10-fold cross validation]	Accuracy: 87.9%
Zhou (70), 2019	LGG, HGG	[IDH wild, IDH mutant with 1p/19q co-deletion, IDH mutant with 1p/19q non-codeletion], [3]	[744], [T1-CE, T2-FLAIR], [TCIA, Local]	[127], [age, histogram, texture, shape]	[RF], [Train-test model]	Accuracy: 78.2% for 3-way classification
Lu (71), 2018	LGG, HGG	[IDH mutant LGG, IDH wild LGG, IDH mutant HGG, IDH wild HGG, IDH mutant LGG + 1p/19q co-deletion], [5]	[284], [T1-CE, T2, T2-FLAIR, DWI], [TCIA for training, Local + REMBRANDT for validation]	[39212], [Shape, size, GLCM texture, LBP texture, first order statistical]	[SVM, Decision Tree], [5-fold cross validation]	Accuracy: 81.1% for 5-way classification, 85.1% for IDH mutant/wild LGG/HGG classification, 89.2% for IDH mutant LGG +1p/19q co-deletion
Li (72), 2018	HGG (Glioblastoma)	[IDH1 mutant, IDH1 wild], [2]	[225], [T1, T2, T1-CE, FLAIR], [TCIA + 3 local hospitals]	[1614], [location, geometry, texture, intensity]	[RF], [Train test model]	Accuracy: 97%
Voort (73), 2019	LGG	[IDH mutant with 1p/19q co-deletion, without co-deletion], [2]	[413], [T1, T2], [TCIA + local medical centers]	[80], [location, intensity, shape, texture, age, sex]	[SVM], [cross validation]	Accuracy: 69.3%
Zhang (74), 2017	Primary HGG (III & IV)	[IDH mutant, IDH wild], [2]	[120], [T1, T1-CE, T2, T2-FLAIR, DWI]	[391], [age, sex, location, shape, volume, intensity, histogram, GLCM texture]	[RF], [Train-test model]	Accuracy: 89%
Yu (75), 2017	LGG (Grade II)	[IDH1 mutant, IDH1 wild], [2]	[110], [T2 FLAIR]	[671], [Location, intensity, shape, texture, Wavelet]	{SVM, Adaboost], [Leave-one-out cross validation]	Accuracy: 80% for both classifiers
Hsieh (76), 2017	HGG (Glioblastoma)	[IDH1 mutant, IDH1 wild], [2]	[39], [T1-CE]	[Morphological, Intensity, texture]	[Logistic regression]	Feature wise Accuracy: 51% for morphological features, 59 % for intensity and 85 % with texture
Zhang (77), 2018	LGG	[IDH mutant with TP53, IDH mutant without TP53, IDH wild], [3]	[103], [T1, T2, T1-CE, FLAIR],	[276], [VASARI, texture, histogram]	[SVM], [train-test model]	Accuracy: 72.8%, 71.9%, 70% for 3 classes
Joo (78), 2019	HGG	[IDH mutant, IDH wild], [2]	[71], [APT]	[APT signal, clinical factors]	[Multivariate cox regression]	APT signal p-value: 0.001

(*continued on next page*)

TABLE 1. (Continued)

Reference Details, Year	Glioma histological Subtype	[Glioma genotype], [No. of classes]	[Sample size], [MRI modality], [dataset]	[No. of features], [Feature list]	[ML method], [Evaluation method]	Performance Testing
Jiang (79), 2017	LGG (grade II)	[IDH mutant, IDH wild], [2]	[27], [APT weighted]	[APT weighted signal]	[ROC-AUC analysis]	AUC: 0.89 for maximum APT value
Jakola (80), 2018	LGG	[IDH mutant, IDH wild], [2]	[25], [FLAIR],	[Volume, Age, GLCM Texture]	[logistic regression]	AUC: 0.940
Bisdas (81), 2018	LGG, HGG	[IDH mutant, IDH wild], [2]	[37], [FLAIR, DKI]	[GLCM Texture, Mean diffusional kurtosis, Skewness]	[SVM]	Accuracy: 83.8 %
Figini (82), 2018	LGG, HGG	[IDH mutant, IDH wild], [2]	[192], [T1, T2, DTI, DKI, NODDI]	[Mean Diffusivity, fractional anisotropy, kurtosis anisotropy, etc]	[statistical analysis]	Accuracy: 79% with fractional anisotropy-max
Eichinger (83), 2017	LGG (II & III)	[IDH mutant, IDH wild], [2]	[79], [DTI]	[101], [LBP texture, volume]	[K-means clustering, ANN]	Accuracy: 92% during training, 95% during validation
Sudre (85), 2019	LGG, HGG	[Grade II, Grade III, Grade IV, IDH mutant, IDH wild], [3]	[333], [T1, T2, FLAIR, DSC MRI], [6 medical centers]	[29], [shape, intensity, texture]	[RF], [cross validation]	Accuracy: 53% for grade classification and 73% for IDH classification
Batchala (98), 2019	LGG (Astrocytoma, Oligodendroglioma)	[IDH mutant with 1p/19q co-deletion, without co-deletion], [2]	[106], [T1, T2, T1-CE, T2-FLAIR]	[Age, texture, T2* signal, location, T2-FLAIR mismatch, hydrocephalus]	[logistic regression]	Accuracy: 86.3%
Kim (99), 2019	LGG, HGG	[IDH mutant with 1p/19q co-deletion, without co-deletion], [2]	[143], [T1, T1-CE, T2, FLAIR], [BRATS 2017 +TCGA]	[479+], [texture, topological, CNN derived features]	[RF, Logistic regression, kTSP], [5-fold cross validation]	Accuracy: 71.4% for RF and 70% for logistic regression
Rathore (102), 2018	HGG (Glioblastoma)	[IDH1, MGMT, EGFRvIII], [3]	[361], [T1, T1-CE, T2, T2-FLAIR, DTI]	[267], [GLCM texture, Volume, intensity, histogram, location, biophysical growth]	[K-means clustering], [10-fold cross validation]	Accuracy: 88%
Rathore (109), 2019	HGG (Glioblastoma)	[GBM subtypes- classical, mesenchymal, proneural, neural] [4]	[112], [T1, T1-CE, T2, T2-FLAIR], [local hospital (HUP)]	[16+], [volume, location, intensity, texture]	[SVM], [5-fold cross validation]	Accuracy: 88.4% for classical, 75.9% for mesenchymal, 82.1% for proneural, 75.9% for neural
Macyszyn (110), 2015	HGG (Glioblastoma)	[GBM subtypes- classical, mesenchymal, proneural, neural] [4]	[134], [T1, T1-CE, T2, T2-FLAIR, DTI, DSC-MRI]	[60], [age, volume, intensity, cell density, microvascularity, diffusion measures]	[SVM]	Accuracy: 75.76% for 4-way molecular classification, 79% for 3-way prognostic classification
Arita (112), 2018	LGG (II & III) (Astrocytoma, Oligodendroglioma)	[IDH1/2 mutant, IDH1/2 mutant with TERT, IDH wild], [3]	[169], [T1, T2, T1-CE, FLAIR]	[110], [location, intensity, shape, texture]	[Regression], [Train test model]	Accuracy: 87% for IDH mutation classification, 74% for 3-way classification

(*continued on next page*)

TABLE 1. (Continued)

Reference Details, Year	Glioma histological Subtype	[Glioma genotype], [No. of classes]	[Sample size], [MRI modality], [dataset]	[No. of features], [Feature list]	[ML method], [Evaluation method]	Performance Testing
Park (118), 2018	LGG (Grade II)	[IDH mutant with 1p/19q co-deletion, without co-deletion, IDH wild], [3]	[215], [T1, T2, T1-CE, FLAIR, DTI],	[26+], [VASARI features]	[Least Absolute Shrinkage and Selection Operator], [10-fold cross validation]	AUC: 0.778 for validation model
Looze (120), 2018	LGG, HGG	[Grade II/III, Grade III/IV, Grade II/IV, IDH mutant, IDH wild], [5]	[[381], [T1, T2, T1-CE, FLAIR, DWI]	[lesion size, cystic change, ADC values, age]	[RF]	AUC: 98% for Grade II/III, 100% for III/IV, 97% for II/IV, 88% for IDH classification
Paech (123), 2018	LGG. HGG	[IDH mutant, IDH wild, MGMT with methylation, MGMT without methylation, LGG, HGG],[6]	[31], [APT]	[APT CEST signal]	[ROC-AUC analysis]	AUC: 91.84% & 97.96% for IDH, 0.78 & 0.83 for grading
Yang (132), 2015	HGG (Glioblastoma)	[GBM subtypes- classical, mesenchymal, proneural, neural] [4]	[T1-CE, T2-FLAIR]	[Texture]	[RF], [Train-test model]	Accuracy: 72% for classical, 70% for mesenchymal, 82% for proneural, 75% for neural, 69% for survival prediction
Lee (136), 2019	HGG (Glioblastoma)	[IDH1 mutant, IDH1 wild], [2]	[123], [T1, T2, T1-CE, FLAIR, PWI, DWI]	[31+], [volume, ADC map, CBV]	[KNN, SVM, RF, Adaboost, decision tree, NB, LDA, gradient boosting]	Accuracy: 66.3% to 83.4%

Abbreviations: SPGR, spoiled gradient recalled sequence; MRS, magnetic resonance spectroscopy; AUC, area under curve; LBPH, local binary pattern histogram; ANN, artificial neural network; RF, random forest; SVM, support vector machine; KNN, k-nearest neighbor; NB, naïve bays; FDA, flexible discriminant analysis; REMBRANDT, The Repository of Molecular Brain Neoplasia Data; GLCM, gray level cooccurrence matrix; ROC-AUC, receiver operating characteristics-area under curve; BRATS, multimodal brain tumor segmentation; kTSP, k-top scoring pair; CEST, chemical exchange saturation transfer.

TABLE 2. Summary on Experimentation and Results of Research Work Using Deep Learning Methods. It Summarizes The State of Art Research Focusing on Radiogenomics Where Deep Learning-Based Algorithms Have Been Employed to Predict the Molecular Subtypes of Glioma. It Provides the Summary Details for Histological Subtypes Used, Genotypes, Number of Classes Used, Number Of Patients, MRI Modalities Used, Dataset Used, Number of Features Extracted, List of Features, Deep Learning Method (DL), Evaluation Method, and Performance Measures. Evaluation was Performed on Freely Online Available and/or Local Datasets

Reference Details, Year	Glioma histological Subtype	[Glioma genotype], [No. of classes]	[Sample size], [MRI modality], [dataset]	[No. of features], [Feature list]	[DL method], [Evaluation method]	Performance testing
Chang (86), 2018	LGG, HGG	[IDH mutant, IDH wild], [2]	[201], [T1, T2, T1-CE, T2-FLAIR], [TCIA and Local]	[Age and Auto-extracted features]	[CNN], [Train test validation model]	Accuracy: 89.1%
Chang (89), 2018	LGG, HGG	[IDH mutant, IDH wild, IDH mutant with 1p/19q co-deletion, IDH mutant with MGMT], [4]	[259], [T1, T2-FLAIR],	[Auto-extracted features, Feature selection with PCA]	[CNN], [train test model]	Accuracy: 94% for IDH, 92% for IDH with 1p/19q co-deletion, and 83% for MGMT status
Liang (90), 2018	LGG, HGG	[IDH mutant, IDH wild], [2]	[167], [T1, T2, T1-CE, T2-FLAIR], [TCGA-BRCA]	[Age, sex, Auto-extracted features]	[CNN], [5-fold cross validation]	Accuracy: 91.4%
Li (91), 2017	LGG (II)	[IDH1 mutant, IDH1 wild], [2]	[119], [T1-CE, T2-Flair],	[16384], [Auto-extracted features]	[CNN], [Leave one out cross validation, SVM]	Accuracy: 94.38%
Banerjee (92), 2019	LGG, HGG	[LGG 1p/19q codeletion positive and negative], [2]	[444], [T1, T1-CE, T2, FLAIR], [BRATS and TCIA]	[Auto-extracted features]	[CNN- PatchNet, SliceNet, VolumeNet]	Accuracy: 97% with VolumeNet for 1p/19q codeletion
Nalawade (94),2019	LGG, HGG	[IDH mutant, IDH wild], [2]	[260], [T2], [TCIA]	[Auto-extracted features]	[CNN – ResNet-50, Inception-v4, DenseNet-161]	Accuracy: 83.8%
Chandan (95), 2019	LGG, HGG	[IDH mutant, IDH wild], [2]	[214], [T1-CE, T2, FLAIR], [TCIA]	[Auto-extracted features]	[CNN]	Accuracy: 97.14% with only T2 data
Ahmad (96), 2019	HGG	[IDH1 mutant, IDH1 wild], [2]	[71], [T2], [Local]	[Auto-extracted features]	[CNN], [4-fold cross validation]	Accuracy: 86.7%
Choi (97), 2019	LGG, HGG	[IDH mutant, IDH wild], [2]	[463], [T1, T2, T1-CE, T2-FLAIR, DSC-MRI],	[Auto-extracted features]	[RNN]	Accuracy: 92.8%
Akkus (100), 2017	LGG (Astrocytoma, Oligodendroglioma, oligoastrocytoma)	[IDH mutant with 1p/19q co-deletion, without co-deletion], [2]	[159], [T1-CE, T2],	[Auto-extracted features]	[CNN], [train test model]	Accuracy: 87.7%

Abbreviations: BRCA, breast invasive carcinoma; PCA, principal component analysis; BRATS, multimodal brain tumor segmentation; RNN, recurrent neural network.

TABLE 3. Summary on Experimentation and Results of Research Work for WHO Grading and Survival Prediction. It Summarizes the Predictive Studies Performed to Assess the Histological Grade of Glioma and Survival Prediction. Histological Grading Classifies the Glioma as Low-grade Glioma (LGG)/High-grade Glioma (HGG) or as per WHO Grade II/III/IV. Survival Prediction Predicts Different Groups for Overall Survival and/or Progression Free Survival Based on Number of Months/Days. Analysis is Performed Either Using Univariate/Multivariate Statistical Analysis or Machine Learning Classifier or Machine Learning Regression Method or Deep Learning-Based Methods. Table Provides the Summary Details for Histological Subtypes Used, Different Classes, Number of Classes Used, Number of Patients, MRI Modalities Used, Dataset Used, Number of Features Extracted, List of Features, Analysis Method, Evaluation Method, and Performance Measures. Performance Measures Used are Accuracy, AUC Value, *p*-Value, Hazard Ratio (HR), Concordance Index

Reference Details, Year	Glioma histological Subtype	[Classes], [No. of classes]	[Sample size], [MRI modality], [dataset]	[No. of features], [Feature list]	[Analysis method], [Evaluation method]	Performance testing
Hwan-Ho (57), 2017	LGG, HGG	[LGG, HGG], [2]	[T1, T2, T1-CE, FLAIR], [BRATS 2015]	[45], [Histogram, shape, GLCM texture]	[Linear regression], [10-fold cross validation]	Accuracy: 89.8%
Bisdas (81), 2018	LGG, HGG	[Grade II as negative, Grade III as positive], [2]	[37], [FLAIR, DKI]	[GLCM Texture, Mean diffusional kurtosis, Skewness]	[SVM], [Train test model]	Accuracy: 75% for WHO grading
Sudre (85), 2019	LGG, HGG	[Grade II, Grade III, Grade IV, IDH mutant, IDH wild], [3]	[333], [T1, T2, FLAIR, DSC MRI], [Local (6 medical centers)]	[29], [shape, intensity, texture]	[RF], [cross validation]	Accuracy: 53% for grade classification and 73% for IDH classification
Tian (119), 2018	LGG, HGG	[LGG, HGG, Grade III, Grade IV], [4]	[153], [T1, T2, T1-CE, DWI, spin labelling]	[510], [histogram, texture, location, volume, histologic subtype]	[SVM]	Accuracy: 96.8% for LGG vs HGG and 98.1% for Grade III vs. IV
Looze (120), 2018	LGG, HGG	[Grade II/III, Grade III/IV, Grade II/IV, IDH mutant, IDH wild], [5]	[381], [T1, T2, T1-CE, FLAIR, DWI]	[lesion size, cystic change, ADC values, age]	[RF]	AUC: 98% for Grade II/III, 100% for III/IV, 97% for II/IV, 88% for IDH classification
Gao (121), 2016	LGG, HGG	[Grade II, III and IV], [3]	[124], [T2 FLAIR], [Local]	[287], [Intensity, shape, wavelet, GLCM texture]	[SVM, Adaboost]	Accuracy: 88.71 % using SVM
Ranjith, (122) 2015	LGG, HGG	[Benign- Grade II, Malignant- Grade III & IV], [2]	[28], [MR Spectroscopy], [local medical institute]	[5], [ratios of 3 metabolites- Creatine, Choline, NAA concentration]	[MLP, SVM, RF, Locally weighted learning], [5-fold cross validation]	AUC: 0.911 using RF method
Paech (123), 2018	LGG. HGG	[IDH mutant, IDH wild, MGMT with methylation, MGMT without methylation, LGG, HGG],[6]	[31], [APT]	[APT CEST signal]	[ROC-AUC analysis]	AUC: 91.84% & 97.96% for IDH, 0.78 & 0.83 for grading with different APT parameters

(*continued on next page*)

TABLE 3. (Continued)

Reference Details, Year	Glioma histological Subtype	[Classes], [No. of classes]	[Sample size], [MRI modality], [dataset]	[No. of features], [Feature list]	[Analysis method], [Evaluation method]	Performance testing
Wiestler (124), 2016	LGG, HGG	[Class1- Grade II/III, Class2- Grade IV], [2]	[37], [T1, T2, DSC-MRI, BOLD]	[116], [contrast enhancement, cerebral blood volume, oxygenation factor]	[RF], [5-fold cross validation]	Accuracy: 91.8% for WHO grade classification for both classes
Wang (125), 2019	LGG, HGG	[Grade II, Grade III, Grade IV], [3]	[146], [Local]	[morphological features, intensity, texture]	[SVM, RF, NN, gradient boosting], [cross validation]	Accuracy: 90% for SVM
Lo (126), 2019	Diffuse gliomas	[Grade II, III and IV], [3]	[130], [T1 axial], [TCIA]	[Auto extracted features]	[CNN], [10-fold cross validation]	Accuracy: 97.9 %
Yang (127), 2018	LGG, HGG	[LGG, HGG], [2]	[113], [T1, T2, T1-CE, FLAIR, DWI, DCE, ASL]	[Auto extracted features]	[CNN- GoogLeNet & AlexNet], [5-fold cross validation]	Accuracy: 90.9% using GoogLeNet
Survival Prediction:						
Wang (58), 2015	HGG (Glioblastoma)	[Overall survival (OS), Progression free survival (PFS)]	[280], [T1, T1-CE, T2], [Local]	[age, sex, KPS, contrast enhancement and patterns, edema, MGMT status, IDH status]	[Univariate, multivariate statistical analysis]	p-value: 0.022 for IDH association with PFS and 0.018 with OS
Kickingereder (104), 2016	HGG (Glioblastoma)	[OS & PFS - low and high-risk groups], [4]	[119], [T1, T1-CE, FLAIR, DWI]	[12190], [first order statistics, volume, shape, texture, clinical data]	[Supervised Principal Component Analysis]	Concordance index: 0.696 for OS, 0.637 for PFS
Macyszyn (110), 2015	HGG (Glioblastoma)	[OS – long, medium, short] [3]	[134], [T1, T1-CE, T2, T2-FLAIR, DTI, DSC-MRI]	[60], [age, volume, intensity, cell density, micro-vascularity, diffusion measures]	[SVM]	Accuracy: 79% for 3-way prognostic classification
Osman (128), 2018	HGG (Glioblastoma)	[OS – long: >18 months, medium: 6 to 18, short: < 6] [3]	[291], [T1, T1-CE, T2, T2-FLAIR], [BRATS 2017]	[age, tumor size, location]	[SVM- regression and classification both]	Accuracy: 0.49 for regression and 1.0 for classification of validation data
Bae (129), 2018	HGG (Glioblastoma)	[OS, PFS – low and high-risk groups], [4]	[217], [T1-CE, T2, T2-FLAIR, DTI], [Local]	[796], [MGMT & IDH status, age, KPS, resection extent, postoperative treatment, texture, shape, ADC histogram	[RSF]	AUC: 0.782 for OS, 0.737 for PFS

(*continued on next page*)

TABLE 3. (Continued)

Reference Details, Year	Glioma histological Subtype	[Classes], [No. of classes]	[Sample size], [MRI modality], [dataset]	[No. of features], [Feature list]	[Analysis method], [Evaluation method]	Performance testing
Jones (130), 2019	LGG of older population (Grade II)	[OS, PFS]	[111], [T2, FLAIR, pre-operative and post-operative MRI], [Local]	[Age, seizure, tumor size, biopsy, chemo-therapy, radiation, IDH status]	[Univariate and bivariate statistical analysis]	Univariate- HR: 0.17 and p-value $<$ 0.001 for IDH association with OS, Bivariate – HR: 0.22 and p-value: 0.008 for age and IDH association with OS
Suchorska (131), 2019	LGG, HGG (Grade II, III)	[OS, PFS – low and high-risk groups], [4]	[301], [T1, axial T2, axial FLAIR, axial DWI], [Local]	[Age, KPS, 1p/19q codeletion status, presence of contrast enhancement (CE), IDH status, WHO grade]	[Univariate and multi variate cox regression analysis, RSF analysis]	Univariate analysis: p-value for association of CE: 0.001 for OS, 0.002 for PFS, RSF Concordance index: 0.859 for OS, 0.704 for PFS
Yang (132), 2015	HGG (Glioblastoma)	[12-month survival status- long, short] [2]	[82], [T1-CE, T2-FLAIR]	[976], [Texture]	[RF], [Train-test model]	Accuracy: 69% for survival prediction
Sun (133), 2019	LGG, HGG	[OS – short ($<$10 months), medium (10-15), long ($>$15 months)], [3]	[442], [T1, T1-CE, T2, T2-FLAIR,], [BRATS 2018]	[14 selected], [Shape, texture, first order statistical]	[RF regression]	Accuracy: 61.0%
Sanghani (134), 2018	HGG (Glioblastoma)	[OS 2-class groups: short ($<$ 400 days) & long ($>$400 days), OS 3-class groups: short ($<$10 months), medium (10 to 15) & long ($>$15)], [2 or 3]	[163], [T1, T1-CE, T2, T2-FLAIR], [BRATS 2017]	[2201], [Texture, shape, volumetric, age]	[SVM], [5-fold cross validation]	Accuracy: 98.7% for 2-class, 88.95% for 3-class
Chaddad (135), 2018	HGG (Glioblastoma)	[OS, PFS – short and long survival], [4]	[40], [T1, FLAIR]	[Texture]	[Univariate analysis – log rank, spearman rank correlation, multivariate RF], [5-fold cross validation]	AUC using RF: 74.38% for OS, 83.5% for PFS
Peeken (140), 2018	HGG (Glioblastoma)	[OS, PFS]	[189], [T1, T1-CE, T2, FLAIR, DWI], [REMBRANDT]	[Age, KPS, gender, MGMT & IDH status, VASARI features]	[Multivariate cox regression]	Concordance index: 0.716 for OS, 0.643 for PFS

(*continued on next page*)

TABLE 3. (Continued)

Reference Details, Year	Glioma histological Subtype	[Classes], [No. of classes]	[Sample size], [MRI modality], [dataset]	[No. of features], [Feature list]	[Analysis method], [Evaluation method]	Performance testing
Chato (141), 2017	LGG, HGG	[OS groups – short (< 10 months), medium (10 to 15 months), long (> 15 months)], [3]	[163], [T1, T1-CE, T2, T2-FLAIR], [BRATS 2017]	[volumetric, intensity, texture, histogram, statistical, deep CNN features]	[SVM, KNN, LDA, logistic regression, CNN]	Accuracy: 73% using LDA
Li (142), 2017	HGG (Glioblastoma)	[OS - low and high-risk groups], [2]	[92], [T1, T1-CE, T2, T2-FLAIR], [Local & TCIA data]	[45792], [Texture at different voxel size, quantization and gray levels]	[Cox regression model]	Concordance index: 0.705
Shboul (143), 2018	HGG (Glioblastoma)	[OS groups – short (< 10 months), medium (10 to 15 months), long (> 15 months)], [3]	[163], [T1, T1-CE, T2, T2-FLAIR], [BRATS 2017]	[1207 extracted, 240 selected], [Texture, volumetric, location, histogram]	[RF regression]	Accuracy: 63%
Han (144), 2020	HGG	[OS – short, long survivor], [2]	[178], [T1-CE], [Local & TCIA data]	[8540], [348 hand crafted – volume, size, texture, intensity, first order statistical + 8192 deep CNN features]	[Elastic net-cox modelling], [Train-test]	Log-rank test p-value < 0.001
Nie (145), 2019	HGG	[OS groups – short (< 650 days), long (> 650 days)], [2]	[68], [T1-CE, DTI, rs-MRI], [Local]	[Age, size, histological type, 3D deep CNN features]	[SVM], [3-fold cross validation]	Accuracy: 90.66%
Lao (146), 2017	HGG (Glioblastoma)	[OS - low and high-risk groups], [2]	[112], [T1, T1-CE, T2, T2-FLAIR], [Local & TCIA data]	[99707 extracted and 150 selected], [1403 hand crafted – texture, intensity, geometrical + 98304 deep CNN features]	[Multivariate cox regression model]	Concordance index: 0.739

Abbreviations: MLP, multi-layer perceptron; NAA, n-acytel aspartate; NN, neural network; RSF, random survival analysis; HR, hazard ratio; KPS, karnofsky performance status; LDA, linear discriminant analysis; rs-MRI, functional resting state MRI.

have illustrated this capability as learning imaging features automatically alleviates the time-consuming preprocessing steps required in radiomics. A variety of CNN architectures have been tested (86−92), however ResNET architecture has been demonstrated to be the most stable and robust in discriminating IDH. The result of deep learning models on multi-modal MRI yielded accuracy 85.7% during testing phase, which was improved up to 89.1% with age as an additional contributing marker (86). Furthermore, to avoid over-fitting, data augmentation techniques have been widely employed while transfer learning was adopted to improve generalizability of the classifier (93). Another recent study employed patch based deep model and demonstrated 97% accuracy in delineating IDH mutation on a mixed data (TCIA and local) (94,95). To gain more interpretability of the CNN, instead of using it as a black-box model, studies have employed class activation mapping − where a map of the most discriminative regions is extracted from the trained model (93,96). A recent study employed convolutional long short-term memory model on perfusion MRI illustrated an accuracy of 92.8% (97). In summary, deep nets with increasing available datasets, demonstrate a future potential for superior predictive models to characterize IDH mutation.

IDH Mutation With 1p/19q

In low grade gliomas, IDH mutation with 1p/19q co-deletion is classified as an oligodendroglioma. It is demonstrated that IDH mutant with 1p/19q codeletion exhibits less aggressive environment than IDH mutant without codeletion (22). In terms of visual features, as described in the earlier section, the T2-FLAIR mismatch sign is of importance as the mismatch indicates IDH mutation with non-codeleted 1p/19q astrocytoma (64). The significant contribution of T2-FLAIR mismatch sign was validated with 100% sensitivity for non-codeleted LGGs (98). Variety of radiomic features such as texture, shape, size, intensity, and histogram have been analyzed for 1p/19q prediction. Out of these, texture quantifiers carried a greater discriminative power in comparison to other attributes (69). Moreover, topological features that quantify shape features or geometrical information such as connected components, rings, cavity, etc. demonstrated higher predictive performance with 5% improvement in accuracy than texture features (99). Integration of age into radiogenomic model contributed substantially and significantly improved the accuracy (70). Furthermore, tumor location also played a vital role in 1p/19q discrimination (97,100). In terms of DL, a recent multi-scale CNN was used by Akkus et al. with 30-fold augmented data that could predict the 1p/19q co-deletion with an accuracy of 87.7% (100).

Epidermal Growth Factor Receptor

Earlier studies on imaging characteristics of EGFR illustrated higher T2/T1 ratio, with quantified enhancement on T1-CE as a potential indication of lack of EGFRvIII mutation as well as perfusion markers to be critical predictors of EGFRvIII mutation (101). Moreover, diffusion and FLAIR markers from solid tumors (uniformly vascularized with small sized edema) were also crucial in delineating EGFRvIII mutation, however were not important in non-uniform types (peritumoral edematous tissue with large irregular shape, with maybe deep but less dense infiltration) (102). Assessment of the EGFRvIII mutation has been performed using radiomics and has demonstrated around 80-85% accuracy of discriminating the EGFRvIII mutation (103). However, other studies contradict such high predictive power as these could achieve accuracies upto only 65% (104). Support vector machine based classifiers were employed in the majority of these studies (102,105) while random forest and stochastic gradient based methods were implemented by Kickingereder et al. (104). Additionally, singular features such as border sharpness coefficients on T2 have been related to EGFR amplification (101). EGFR prediction has not yet been performed using any deep models.

Methyl-guanine Methyl Transferase (MGMT)

Recently, radiomics has also been applied for MGMT status prediction on multi-modal MRI (T1-CE, T1, T2, and FLAIR) in gliomas. The predictive accuracies from multiple studies have varied between 61% and 80% on cohorts ranging between 82 and 193 subjects (104,106,107). Hajinafar et al. applied an adaboost based classification framework and reported that the Laplacian of Gaussian (LOG) filter in edema single-handedly could discriminate MGMT status with 0.78 AUC (106). Li et al. used a Boruta algorithm to rank the features and employed a random forest classifier to illustrate that texture features on the whole tumor and specifically found that Gray Level Size Zone Matrix of low grey level emphasis could delineate the MGMT with an AUC of 0.71 (107). Kickingereder et al. in addition to T1-CE, T2, T1, and FLAIR also used perfusion images and demonstrated that higher Gaussian-normalized relative CBV (nrCBV) in T1-CE as well as higher ratio of contrast enhancing tumor to complete tumor volume were the most crucial features for identifying MGMT (104) . The prediction of IDH genotype, 1p/19q codeletion status and MGMT promotor methylation in both high- and low-grade gliomas illustrated high accuracies using deep CNN. Each genomic type showed distinct imaging features such as definition of tumor margins, T1 and FLAIR suppression, amount of edema, amount of necrosis, and textural features (108).

Transcriptomic Delineation of Glioblastomas (GBMs)

The four molecular subtypes of classical, mesenchymal, proneural and neural as described by Verhaak et al. can also be identified using radiomics based framework (27). Recent works have demonstrated approximately 71% to 76% accuracies in delineating these four subtypes using T1, T1-CE, T2, and FLAIR in Rathore et al. and in addition using DTI and DSC MRI in Macyszyn et al. (109,110). Both the studies relied on support vector machines (SVMs) where one

demonstrated four distinct MRI phenotypes based on volume of different regions of tumor and intensity distributions of those regions (110) while Rathore et al. illustrated low T1-CE signal and high FLAIR signal in edema in proneural and neural subtypes respectively. Classical subtype was associated with edge sharpness of the edema region as delineated from multi-modal MRI images while mesenchymal correlated with higher T2 and FLAIR signal in edema and higher volume of enhancement on T1-CE.

Other genotypes

Multiple common mutations in gliomas such as TERT promoter (111), TP53, ATRX, phosphatidylinositol-4, 5-bisphosphate 3-kinase catalytic subunit alpha (PIK3CA), phosphatidylinositol-4, 5-bisphosphate 3-kinase regulatory subunit 1 (PIK3R1), $BRAF^{V600}$, histone 3-lysine-27-methionine (H3K27M) etc. are changing the current view of glioma diagnosis. Glioma patients with unmethylated MGMT and TERT promoter mutation have poor prognosis than those with wild-type TERT (112). Preoperative detection of TERT promoter mutation is useful in patients with glioblastoma as it may help in selecting patients for therapeutic strategies such as telomerase-targeted therapies (112). Oligodendroglioma and astrocytoma having mutations in IDH with TERT promoter are uniquely located in medial frontal cortex region and radiomic features were able to discriminate IDH1/2-mutant, IDH1/2-mutant with TERT promoter mutation, and IDH-wild type with high accuracy (81). Moreover, a recent study employed CNNs to discriminate TERT promotor genotype in LGGs and illustrated a high accuracy of 84.0% (113).

Most infiltrating high grade gliomas, especially secondary glioblastoma, have novel alteration in TP53 along with IDH mutation (114) whereas the significant differences with 85% accuracy were found in low grade gliomas for IDH and TP53 status prediction (115). Prediction of ATRX on TCIA data could be achieved with an accuracy of 72.5% where features such as sum average and variance were highly discriminative on T2-weighted images (116). H3K27M, which is the most frequent mutation in brainstem gliomas was accurately classified using radiomics (84.4%) with edge and texture features as the most delineating attributes (117).

Grading

The prediction of histological tumor-grade as specified by WHO is being investigated from several years to understand its severity invasively as well as non-invasively. Even though the recent recommendations as per WHO rely more on tumor genomic profile, histologic grading is a vital phenotypic measure. Gliomas are either discriminated into grade II, III and IV (118) or as LGG or high grade gliomas (HGG) (59,119). Features such as necrotic core, T1-CE enhancement, localization in supra-tentorial white matter define glioblastoma. However, these have significant variability in size with infiltration that is present beyond the visible tumor. For LGGs, the imaging features such isointense/hypointense T1, as T2-FLAIR mismatch etc. as crucial in identifying the grade. Combined grade differentiations (II-III / III-IV / II-IV) have been driven by different radiographic features such as shape, texture, volume, intensity etc. (85,120). T1-CE could well predict the difference between LGG and HGG with accuracy 89% by analyzing selected set of histograms and Gray-Level Co-occurrence Matrix features (57). Around 287 features from single T2-FLAIR modality were analyzed to decide the grade of glioma (121). Structural as well as advanced MRI methods such as blood oxygen level dependent, perfusion imaging, diffusion imaging, MR spectroscopy has been evaluated for grade prediction. The features from MR spectroscopy substantially improved the noninvasive classification of glioma into benign with Grade II and malignant with Grade III-IV yielding AUC up to 0.92 (122). The performance of structural (T1-CE, T2) and diffusion modality (ADC) was better than perfusion MRI (CBFs) to classify glioma into LGG and HGG. Furthermore, T1-CE and ADC contributed significantly to discriminate Grade III and IV (119). Moreover, grade discrimination between grade II and grade III was better achieved from diffusion kurtosis imaging (DKI) features than T2-FLAIR features (81). Delineation of LGGs from HGGs has been enabled by APT (amide proton transfer) measures with an AUC 0.78 (123). Overall, very high accuracies of up to 98% have been achieved for grade classification using multimodal analysis (119,120,124,125). Furthermore, deep convolutional neural network with pre-trained weights have also been employed in automated grading of gliomas (126,127).

Survival Prediction

The survival associations are well predicted with various molecular markers suggesting the varying degrees of prognostic impact. Overall survival (OS), progression free survival (PFS) are examined with molecular analysis from 12-months to 120-months survival period. These survival periods are classified into two to three classes like short survival (less than 6 months), medium survival (6−18 months), long survival (more than 18 months) (128). Radiomic phenotyping has shown to improve the performance of survival prediction model when integrated with clinical, pathological and genetic profiles (129). IDH mutations have revealed better survival prediction than IDH wildtype in LGGs as well as HGGs (58,114,130,131). Furthermore, IDH mutation with 1p/19q codeletion have improved impact on glioma prognosis (21,131), which consequently may improve the survival outcomes. Attributes such as voxel size, volume, texture, shape, intensity etc. from multimodality datasets have been of utmost importance in predicting survival (132,104,133). Amongst these features, quantification of contrast enhancement has been a crucial marker (131). Information on IDH mutation significantly impacts the classification as mutant status is more discriminative than the age of the patient and

even for older patients demonstrates comparatively higher survival. (110,130). Recent literature also demonstrates various other features that are critical in survival prediction. For example, Sanghani et al. demonstrated that 2D shape features contribute more to determine the survival rate of GBM patients (134). Dalu Yang et al. analyzed that texture features are more effective in GBM characterization to assess 12-months survival status (132). Chaddad et al. illustrated that features extracted from edema and active tumor region are highly associated with overall survival of GBM whereas the texture features of edema region strongly correlate with PFS (135). Incorporating diffusion and perfusion MRI into radiomic model has also shown to improve the performance of GBM survival analysis (136).

VASARI (Visually AcceSAble Rembrandt Images) MRI feature set (137−139) is a widely adopted feature set which consists of 24 observations familiar to neuroradiologists, to describe the morphology of brain tumors. Peeken et al. show significant association of VASARI features like deep white-matter invasion, multilocality, satellites, and ependymal invasion with progression free survival and overall survival of GBM patients (140).

CNN based methods are also being adopted for survival prediction (141−143). Deep features are usually extracted from final layer(s) of pre-trained CNN models (144). A SVM based feature analysis framework which combines deep features with radiomics features achieved an accuracy of 90.66% for survival prediction (144,145). Lao et. al demonstrated that the performance of deep features and radiomics features is further improved by incorporating clinical factors like age and Karnofsky performance score (KPS) (146).

Challenges

The emerging, non-invasive area of radiogenomics illustrates enormous potential in genomic profiling, grading and subtyping of gliomas based on multi-modal MRI. The techniques demonstrate prospective possibilities of overcoming inaccuracies in tissue sampling, as it considers the complete spatial extent of the tumor. Nonetheless, multiple challenges that need to be accounted for while building the computation framework and during interpreting results are given below.

Abundant Data Availability

To build more generalized and robust models, it is crucial to train these on ample amount of data with sufficient variability. This is more important in training DL algorithms as with petite datasets, these tend to overfit and although may provide remarkable training accuracies, will fail on external testing data.

Creating large open to public datasets for benchmarking machine learning and DL based algorithms has therefore become crucial as AI techniques require large amounts of data to learn the underlying patterns for creation of robust models. Usually, it is difficult for a single site to create large amounts of data and therefore pooling data from multiple sites is highly desirable. These datasets not only support progress in research but also provide a baseline to test the sensitivity and precision of the developed algorithms. To this end, the Cancer Genome Atlas (TCGA) has made cancer datasets publicly available with the comprehensive catalogue of genomic profiles. The TCIA [https://www.cancerimagingarchive.net/] includes a large updated collection of cancer images accessible for public to download. The DICOM (Digital Imaging and Communications in Medicine) images of different modalities (MRI, computed tomography (CT), etc.) related to specific cancer type are provided along with other auxiliary data such as genomic profile, patient profile, demographics, treatment information, outcomes, etc. (147). The TCIA data has a small representation of brain tumors (700) where around 50% of these are gliomas with multi-modal MRI and information on genotypes, demographics and survival in many cases. A sub-set of this data has been robustly preprocessed by Bakas. et al. (148) for direct usage in developing algorithms.

Inter-scanner variability

Radiomics may vary significantly based on the MRI machine, the magnet strength, homogeneity, and acquisition parameters (149). It is therefore crucial to account for such inter-scanner diversity while using the data driven radio-phenotypic characterizations. Although models are trained using datasets from multiple scanners for more generalizability, leave-one-site-out type analysis creating uncertainties about the adaptability to unseen datasets acquired from different scanners with diverse scanning protocols has not been performed.

To this end, data harmonization techniques could play an important role in radiogenomic analysis. Harmonization has been employed frequently in analysis of psychiatric and neuro-degenerative diseases on multi-site diffusion and functional MRI images (150). Moreover, methods have also been developed to harmonize brain connectomes (networks) (151). On similar lines, advances in harmonizing radiomics is a crucial problem that needs to be addressed. With DL methods, the underlying assumption is that the model will learn the inherent differences between the scanners and finally only focus on the radiophenotypic discriminative patterns. However, to substantiate this assumption leave- one-site-out type studies are binding.

Pre-processing and Segmentation

Preprocessing methods include brain extraction, denoising, histogram matching, intra-subject registration, registration to a template, multi-modal tumor segmentation, and radiomic feature extraction. In DL based techniques the final two steps are generally not required. A variety of data preprocessing routines and varying criteria to segment and to compute radiomics adds to the challenge of consistency and

standardization. Furthermore, the varying parametrization could stem from the quality of datasets itself. For example, datasets from some scanners may be noisier than others and may require additional preprocessing such as denoising. It is therefore crucial to well document the acquisition protocols, and the preprocessing pipelines in detail. Efforts by groups such as Bakas et al. (148) have made preprocessed data available for benchmarking novel computational methods. The preprocessing technique is described in detail so that it can be adapted by other groups. This could be a potential approach to alleviate this challenge. In DL based methods, since preprocessing steps are limited, the variability in methods is of lesser concern.

Over-fitting

While using multi-variate models with radiomics, many studies employ higher number of radiomic features than the number of samples, which leads to a commonly known issue of 'curse of dimensionality' that overfits the training data. The overfitting reduces the robustness and generalizability of the classifier and such classifier often fails while testing new data. In terms of radiomic studies, feature selection can alleviate this issue as it removes unwanted features and retains the most discriminative/un-correlated ones. In DL based model, a similar problem is encountered with lesser number of training samples as DL uses millions of auto-extracted features. To mitigate this problem, the best solution is to have ample data. In case big datasets are not available it is recommended to not rely on DL based training algorithms.

Finally, in both these cases to establish the working of the model, it is vital to perform n-fold cross-validation and external testing. Cross-validation quantitatively validates the performance of the model using various groups of test subjects in a statistically robust manner, while external testing facilitates potential of usage in the clinical workflow.

Interpretability

Clinical interpretability is of utmost importance to gain deeper understanding of which radio-phenotypical features relate to a certain genotype. Evidence from multiple studies can support connections between radiographic signatures and underlying genetic changes and consequently can be used in clinical practice (152,153). The most discriminative radiomic features computed by a certain statistical ranking method, can assist in facilitating novel insights. However, with DL, despite precise performance of CNNs, it remains a black-box model (134,38). Especially, with limited sample size and where the classes cannot be visually discerned, gaining clarity of the CNN operation is particularly imperative, as although the model achieves a good classification performance, it could be susceptible to over-fitting. Attaining insight into the imaging features and regions that are responsible for the delineation is crucial for clinical explain ability. A few recent studies have employed class activation maps to demonstrate which areas of the image significantly participate in the classification. From the study by Chougule et al. it can be observed that the discriminative maps for IDH wildtype cases focus heavily on the T1-CE enhancement (93). Other methods such as attention maps etc. have also been employed with DL (65,154).

Retrospective and Prospective Validations

Majority of the studies published till now provide a prototype model for classification. However, these studies do not take a step forward in validating the model on external retrospective data followed by prospective validation. The need of the hour is to cross-validate these models sufficiently using multi-center, multi-region (geographical location-wise) variety of data to test the generalizability. One recent study attempted to test local cohorts on a TCIA trained model and demonstrated that despite 95% accuracy on TCIA, the testing on local data was futile. It could only provide reasonable results after transfer learning from TCIA model to the local data and then testing the remaining local data (93). Usage of techniques such as federated learning could support in comprehensive validation (155).

CONCLUSION

Advances in quantification of imaging phenotypes to delineate tumor genotypes have been prevalent in the past few years. The utilization of such prognostic markers may not only enhance the radiology workflow but also provide timely and personalized treatment plan for the patient which may consequently lead to better outcomes. However, for such technology to translate into the clinic, it is crucial to closely examine the quantum of recent works and gain insights obstacles and challenges that may be presented. Our work elaborated on all the recent work in classifying glioma genotypes using data driven approaches and discussed the challenges of scanner variability, benchmark datasets as well as aggressive retrospective and prospective testing of models. In summary, current techniques lend credence to future computer aided diagnostics for glioma genotype.

REFERENCES

1. Ostrom QT, Bauchet L, Davis FG, et al. The epidemiology of glioma in adults: a "state of the science" review. Neuro Oncol 2014; 16(7):896–913.
2. Rasmussen BK, Hansen S, Laursen RJ, et al. Epidemiology of glioma: clinical characteristics, symptoms, and predictors of glioma patients grade I-IV in the the Danish Neuro-Oncology Registry. J Neuro Oncol 2017; 135(3):571–579.
3. Munshi A, Jalali R. Therapy for glioma: Indian perspective. Indian J Cancer.` 2009; 46(2):127.
4. Omuro A, DeAngelis LM. Glioblastoma and other malignant gliomas: a clinical review. Jama 2013; 310(17):1842–1850.
5. Daumas-Duport C. Histological grading of gliomas. Curr Opin Neurol Neurosurg 1992; 5(6):924–931.
6. Kleihues P, Soylemezoglu F, Schauble B, et al. Histopathology, classification, and grading of gliomas. Glia 1995; 15(3):211–221.
7. Davis ME. Glioblastoma: Overview of Disease and Treatment. Clin J Oncol Nurs 2016; 20(5 Suppl):S2–S8.
8. Foote MB, Papadopoulos N, Diaz Jr LA. Genetic classification of gliomas: refining histopathology. Cancer cell 2015; 28(1):9–11.

9. Ohgaki H, Kleihues P. Population-based studies on incidence, survival rates, and genetic alterations in astrocytic and oligodendroglial gliomas. J Neuropathol Exp Neurol 2005; 64(6):479–489.
10. Smith JS, Jenkins RB. Genetic alterations in adult diffuse glioma: occurrence, significance, and prognostic implications. Front Biosci 2000; 5: D213–D231.
11. Louis DN, Perry A, Reifenberger G, et al. The 2016 World Health Organization classification of tumors of the central nervous system: a summary. Acta neuropathologica 2016; 131(6):803–820.
12. Cohen AL, Holmen SL, Colman H. IDH1 and IDH2 mutations in gliomas. Curr Neurol Neurosci Rep. 2013; 13(5):345.
13. Olar A, Wani KM, Alfaro-Munoz KD, et al. IDH mutation status and role of WHO grade and mitotic index in overall survival in grade II-III diffuse gliomas. Acta Neuropathol 2015; 129(4):585–596.
14. SongTao Q, Lei Y, Si G, et al. IDH mutations predict longer survival and response to temozolomide in secondary glioblastoma. Cancer Sci 2012; 103(2):269–273.
15. Reitman ZJ, Yan H. Isocitrate dehydrogenase 1 and 2 mutations in cancer: alterations at a crossroads of cellular metabolism. Natl Cancer Inst. 2010; 102(13):932–941.
16. Yan H, Parsons DW, Jin G, et al. IDH1 and IDH2 mutations in gliomas. N Engl J Med. 2009; 360(8):765–773.
17. Dang L, White DW, Gross S, et al. Cancer-associated IDH1 mutations produce 2-hydroxyglutarate. Nature 2009; 462(7274):739–744.
18. Lu C, Ward PS, Kapoor GS, et al. IDH mutation impairs histone demethylation and results in a block to cell differentiation. Nature 2012; 483 (7390):474–478.
19. Huang J, Yu J, Tu L, et al. Isocitrate dehydrogenase mutations in glioma: From basic discovery to therapeutics development. Frontiers in oncology 2019; 9:506.
20. Waitkus MS, Diplas BH, Yan H. Isocitrate dehydrogenase mutations in gliomas. Neuro Oncol 2015; 18(1):16–26.
21. Hu N, Richards R, Jensen R. Role of chromosomal 1p/19q co-deletion on the prognosis of oligodendrogliomas: A systematic review and meta-analysis. Interdisciplinary Neurosurgery 2016; 5:58–63.
22. Boots-Sprenger SH, Sijben A, Rijntjes J, et al. Significance of complete 1p/19q co-deletion, IDH1 mutation and MGMT promoter methylation in gliomas: use with caution. Modern Pathology 2013; 26 (7):922–929.
23. Idbaih A, Marie Y, Pierron G, et al. Two types of chromosome 1p losses with opposite significance in gliomas. Annals of neurology 2005; 58(3):483–487.
24. Beck S, Jin X, Sohn YW, et al. Telomerase activity-independent function of TERT allows glioma cells to attain cancer stem cell characteristics by inducing EGFR expression. Mol Cells 2011; 31(1):9–15.
25. Eckel-Passow JE, Lachance DH, Molinaro AM, et al. Glioma Groups Based on 1p/19q, IDH, and TERT Promoter Mutations in Tumors. N Engl J Med 2015; 372(26):2499–2508.
26. von Deimling A, Korshunov A, Hartmann C. The next generation of glioma biomarkers: MGMT methylation, BRAF fusions and IDH1 mutations. Brain Pathol 2011; 21(1):74–87.
27. Verhaak RG, Hoadley KA, Purdom E, et al. Integrated genomic analysis identifies clinically relevant subtypes of glioblastoma characterized by abnormalities in PDGFRA, IDH1, EGFR, and NF1. Cancer cell 2010; 17 (1):98–110.
28. Kannan K, Inagaki A, Silber J, et al. Whole-exome sequencing identifies ATRX mutation as a key molecular determinant in lower-grade glioma. Oncotarget 2012; 3(10):1194–1203.
29. Zheng H, Ying H, Yan H, et al. p53 and Pten control neural and glioma stem/progenitor cell renewal and differentiation. Nature 2008; 455 (7216):1129–1133.
30. Kreth S, Thon N, Kreth FW. Epigenetics in human gliomas. Cancer letters 2014; 342(2):185–192.
31. Horbinski C, Kofler J, Kelly LM, et al. Diagnostic use of IDH1/2 mutation analysis in routine clinical testing of formalin-fixed, paraffin-embedded glioma tissues. J Neuropathol Exp Neurol. 2009; 68(12):1319–1325.
32. Nassiri F, Zadeh G, Aldape K. IDH mutation testing in gliomas—where do we draw the line? Oxford University Press US, 2017.
33. Aum DJ, Kim DH, Beaumont TL, et al. Molecular and cellular heterogeneity: the hallmark of glioblastoma. Neurosurgical focus 2014; 37(6): E11.
34. Saenz-Antoñanzas A, Auzmendi-Iriarte J, Carrasco-Garcia E, et al. Liquid biopsy in glioblastoma: opportunities, applications and challenges. Cancers 2019; 11(7):950.
35. Fathi Kazerooni A, Bakas S, Saligheh Rad H, et al. Imaging signatures of glioblastoma molecular characteristics: A radiogenomics review. J Magn Reson Imaging 2019.
36. Ferris J, Chang PD, Chow DS. Radiomics and Machine Learning, in Glioma Imaging. Springer, 2020:241–249.
37. Jin W, Fatehi M, Abhishek K, et al., Applying Artificial Intelligence to Glioma Imaging: Advances and Challenges. arXiv preprint arXiv:1911.12886, 2019.
38. Bodalal Z, Trebeschi S, Nguyen-Kim TDL, et al. Radiogenomics: bridging imaging and genomics. Abdom Radiol 2019; 44(6):1960–1984.
39. Mazurowski MA. Radiogenomics: what it is and why it is important. J Am Coll Radiol. 2015; 12(8):862–866.
40. Grover VP, Tognarelli JM, Crossey MM, et al. Magnetic resonance imaging: principles and techniques: lessons for clinicians. J Clin Exp Hepatol. 2015; 5(3):246–255.
41. Ismail AAO, Parker D, Hernandez-Fernandez M, et al. Characterizing peritumoral tissue using DTI-Based free water elimination. International MICCAI Brainlesion Workshop. Springer, 2018.
42. Pasternak O, Sochen N, Gur Y, et al. Free water elimination and mapping from diffusion MRI. Magn Reson Med 2009; 62(3):717–730.
43. Zhang H, Schneider T, Wheeler-Kingshott CA, et al. NODDI: practical in vivo neurite orientation dispersion and density imaging of the human brain. Neuroimage 2012; 61(4):1000–1016.
44. Barajas Jr RF, Cha S. Benefits of dynamic susceptibility-weighted contrast-enhanced perfusion MRI for glioma diagnosis and therapy. CNS oncology 2014; 3(6):407–419.
45. Choi SH, Jung SC, Kim KW, et al. Perfusion MRI as the predictive/prognostic and pharmacodynamic biomarkers in recurrent malignant glioma treated with bevacizumab: a systematic review and a time-to-event meta-analysis. J Neurooncol 2016; 128(2):185–194.
46. Khalifa F, Soliman A, El-Baz A, et al. Models and methods for analyzing DCE-MRI: A review. Medical physics 2014; 41(12):124301.
47. Telischak NA, Detre JA, Zaharchuk G. Arterial spin labeling MRI: clinical applications in the brain. J Magn Reson Imaging 2015; 41(5):1165–1180.
48. Zhou J, Lal B, Wilson DA, et al. Amide proton transfer (APT) contrast for imaging of brain tumors. Magnetic Resonance in Medicine: An Official Journal of the International Society for Magnetic Resonance in Medicine 2003; 50(6):1120–1126.
49. Zhou J, Blakeley JO, Hua J, et al. Practical data acquisition method for human brain tumor amide proton transfer (APT) imaging. Magn Reson Med 2008; 60(4):842–849.
50. Van Griethuysen JJ, Fedorov A, Parmar C, et al. Computational radiomics system to decode the radiographic phenotype. Cancer research 2017; 77(21):e104–e107.
51. Kumar V, Gu Y, Basu S, et al. Radiomics: the process and the challenges. Magn Reson Imaging 2012; 30(9):1234–1248.
52. Narang S, Lehrer M, Yang D, et al. Radiomics in glioblastoma: current status, challenges and potential opportunities. Transl Cancer Res 2016; 5(4):383–397.
53. Chaddad A, Kucharczyk MJ, Daniel P, et al. Radiomics in glioblastoma: current status and challenges facing clinical implementation. Front Onco 2019; 9.
54. LeCun Y, Bengio Y, Hinton G. Deep learning. nature 2015; 521 (7553):436–444.
55. Krizhevsky A, Sutskever I, Hinton GE. Imagenet classification with deep convolutional neural networks. In: Advances in neural information processing systems; 2012.
56. Wu S, Meng J, Yu Q, et al. Radiomics-based machine learning methods for isocitrate dehydrogenase genotype prediction of diffuse gliomas. J Cancer Res Clin Oncol 2019; 145(3):543–550.
57. Hwan-Ho C, Hyunjin P. Classification of low-grade and high-grade glioma using multi-modal image radiomics features. Conf Proc IEEE Eng Med Biol Soc 2017; 2017:3081–3084.
58. Wang K, Wang Y, Fan X, et al. Radiological features combined with IDH1 status for predicting the survival outcome of glioblastoma patients. Neuro Oncol 2015; 18(4):589–597.
59. Qi S, Yu L, Li H, et al. Isocitrate dehydrogenase mutation is associated with tumor location and magnetic resonance imaging characteristics in astrocytic neoplasms. Oncol Lett. 2014; 7(6):1895–1902.
60. Sonoda Y, Shibahara I, Kawaguchi T, et al. Association between molecular alterations and tumor location and MRI characteristics in anaplastic gliomas. Brain Tumor Pathol. 2015; 32(2):99–104.

61. Villanueva-Meyer JE, Wood MD, Choi BS, et al. MRI features and IDH mutational status of grade II diffuse gliomas: impact on diagnosis and prognosis. AJR Am J Roentgenol. 2018; 210(3):621–628.
62. Ding H, Huang Y, Li Z, et al. Prediction of IDH Status Through MRI Features and Enlightened Reflection on the Delineation of Target Volume in Low-Grade Gliomas. Technol Cancer Res Treat. 2019; 18:1533033819877167.
63. Wang Q, Zhang J, Li F, et al. Diagnostic performance of clinical properties and conventional magnetic resonance imaging for determining the IDH1 mutation status in glioblastoma: a retrospective study. PeerJ 2019; 7:e7154.
64. Goyal A, Yolcu YU, Goyal A, et al. The T2-FLAIR–mismatch sign as an imaging biomarker for IDH and 1p/19q status in diffuse low-grade gliomas: a systematic review with a Bayesian approach to evaluation of diagnostic test performance. Neurosurgical focus 2019; 47(6):E13.
65. Broen MP, Smits M, Wijnenga MM, et al. The T2-FLAIR mismatch sign as an imaging marker for non-enhancing IDH-mutant, 1p/19q-intact lower-grade glioma: a validation study. Neuro Oncol 2018; 20 (10):1393–1399.
66. Foltyn M, Nieto Taborda KN, Neuberger U, et al. T2/FLAIR-mismatch sign for noninvasive detection of IDH-mutant 1p/19q non-codeleted gliomas: validity and pathophysiology. Neuro-Oncology Advances 2020; 2(1).
67. Xing Z, Yang X, She D, et al. Noninvasive assessment of IDH mutational status in World Health Organization grade II and III astrocytomas using DWI and DSC-PWI combined with conventional MR imaging. American Journal of Neuroradiology 2017; 38(6):1138–1144.
68. Leu K, Ott GA, Lai A, et al. Perfusion and diffusion MRI signatures in histologic and genetic subtypes of WHO grade II–III diffuse gliomas. Journal of neuro-oncology 2017; 134(1):177–188.
69. Jagtap J, Saini J, Santosh V, et al. Predicting the Molecular Subtypes in Gliomas Using T2-Weighted MRI. In: In: Proceedings of the 2nd International Conference on Data Engineering and Communication Technology, Springer; 2019.
70. Zhou H, Chang K, Bai HX, et al. Machine learning reveals multimodal MRI patterns predictive of isocitrate dehydrogenase and 1p/19q status in diffuse low-and high-grade gliomas. J Neurooncol 2019; 142(2):299–307.
71. Lu CF, Hsu FT, Hsieh KL, et al. Machine Learning-Based Radiomics for Molecular Subtyping of Gliomas. Clin Cancer Res 2018; 24(18):4429–4436.
72. Li ZC, Bai H, Sun Q, et al. Multiregional radiomics profiling from multiparametric MRI: Identifying an imaging predictor of IDH1 mutation status in glioblastoma. Cancer Med 2018; 7(12):5999–6009.
73. van der Voort SR, Incekara F, Wijnenga MMJ, et al. Predicting the 1p/19q Codeletion Status of Presumed Low-Grade Glioma with an Externally Validated Machine Learning Algorithm. Clin Cancer Res 2019; 25 (24):7455–7462.
74. Zhang B, Chang K, Ramkissoon S, et al. Multimodal MRI features predict isocitrate dehydrogenase genotype in high-grade gliomas. Neuro Oncol 2017; 19(1):109–117.
75. Yu J, Shi Z, Lian Y, et al. Noninvasive IDH1 mutation estimation based on a quantitative radiomics approach for grade II glioma. Eur Radiol 2017; 27(8):3509–3522.
76. Hsieh KL, Chen CY, Lo CM. Radiomic model for predicting mutations in the isocitrate dehydrogenase gene in glioblastomas. Oncotarget 2017; 8(28):45888–45897.
77. Zhang X, Tian Q, Wang L, et al. Radiomics Strategy for Molecular Subtype Stratification of Lower-Grade Glioma: Detecting IDH and TP53 Mutations Based on Multimodal MRI. J Magn Reson Imaging 2018; 48 (4):916–926.
78. Joo B, Han K, Ahn S, et al. Amide proton transfer imaging might predict survival and IDH mutation status in high-grade glioma. Eur Radiol 2019; 29:1–10.
79. Jiang S, Zou T, Eberhart CG, et al. Predicting IDH mutation status in grade II gliomas using amide proton transfer-weighted (APTw) MRI. Magn Reson Med 2017; 78(3):1100–1109.
80. Jakola AS, Zhang YH, Skjulsvik AJ, et al. Quantitative texture analysis in the prediction of IDH status in low-grade gliomas. Clin Neurol Neurosurg 2018; 164:114–120.
81. Bisdas S, Shen H, Thust S, et al. Texture analysis-and support vector machine-assisted diffusional kurtosis imaging may allow in vivo gliomas grading and IDH-mutation status prediction: a preliminary study. Sci Rep 2018; 8(1):1–9.
82. Figini M, Riva M, Graham M, et al. Prediction of isocitrate dehydrogenase genotype in brain gliomas with MRI: single-shell versus multishell diffusion models. Radiology 2018; 289(3):788–796.
83. Eichinger P, Alberts E, Delbridge C, et al. Diffusion tensor image features predict IDH genotype in newly diagnosed WHO grade II/III gliomas. Sci Rep 2017; 7(1):1–9.
84. Kang Y, Choi SH, Kim Y-J, et al. Gliomas: Histogram Analysis of Apparent Diffusion Coefficient Maps with Standard- or High-b-Value Diffusion-weighted MR Imaging—Correlation with Tumor Grade. Radiology 2011; 261(3):882–890.
85. Sudre C, Panovska-Griffiths J, Sanverdi E, et al. Machine learning assisted DSC-MRI radiomics as a tool for glioma classification by grade and mutation status. medRxiv 2019:19007898.
86. Chang K, Bai HX, Zhou H, et al. Residual convolutional neural network for the determination of IDH status in low-and high-grade gliomas from MR imaging. Clin Cancer Res. 2018; 24(5):1073–1081.
87. Prasath VS. Deep learning based computer-aided diagnosis for neuroimaging data: focused review and future potential. Neuroimmunol Neuroinflammation 2018; 5:1.
88. Tandel GS, Biswas M, Kakde OG, et al. A review on a deep learning perspective in brain cancer classification. Cancers 2019; 11(1):111.
89. Chang P, Grinband J, Weinberg BD, et al. Deep-Learning Convolutional Neural Networks Accurately Classify Genetic Mutations in Gliomas. AJNR Am J Neuroradiol. 2018; 39(7):1201–1207.
90. Liang S, Zhang R, Liang D, et al. Multimodal 3D DenseNet for IDH Genotype Prediction in Gliomas. Genes (Basel) 2018; 9(8).
91. Li Z, Wang Y, Yu J, et al. Deep Learning based Radiomics (DLR) and its usage in noninvasive IDH1 prediction for low grade glioma. Sci Rep 2017; 7(1):5467.
92. Banerjee, S., S. Mitra, F. Masulli, et al., Deep Radiomics for Brain Tumor Detection and Classification from Multi-Sequence MRI. 2019.
93. Chougule T, Shinde S, Santosh V, et al. On Validating Multimodal MRI Based Stratification of IDH Genotype in High Grade Gliomas Using CNNs and Its Comparison to Radiomics. International Workshop on Radiomics and Radiogenomics in Neuro-oncology. Springer, 2019.
94. Nalawade S, Murugesan GK, Vejdani-Jahromi M, et al. Classification of brain tumor isocitrate dehydrogenase status using MRI and deep learning. J Med Imaging (Bellingham). 2019; 6(4):046003.
95. Bangalore Yogananda CG, Shah BR, Vejdani-Jahromi M, et al. A novel fully automated MRI-based deep-learning method for classification of IDH mutation status in brain gliomas. Neuro Oncol 2019.
96. Ahmad A, Sarkar S, Shah A, et al. Predictive and discriminative localization of IDH genotype in high grade gliomas using deep convolutional neural nets. In: 2019 IEEE 16th International Symposium on Biomedical Imaging (ISBI 2019), IEEE; 2019.
97. Choi KS, Choi SH, Jeong B. Prediction of IDH genotype in gliomas with dynamic susceptibility contrast perfusion MR imaging using an explainable recurrent neural network. Neuro Oncol 2019; 21(9):1197–1209.
98. Batchala P, Muttikkal T, Donahue J, et al. Neuroimaging-based classification algorithm for predicting 1p/19q-codeletion status in IDH-mutant lower grade gliomas. AJNR Am J Neuroradiol 2019; 40(3):426–432.
99. Kim D, Wang NC, Ravikumar V, et al. Prediction of 1p/19q Codeletion in Diffuse Glioma Patients Using Preoperative Multiparametric Magnetic Resonance Imaging. Front Comput Neurosci. 2019; 13:52.
100. Akkus Z, Ali I, Sedlá J, et al. Predicting deletion of chromosomal arms 1p/19q in low-grade gliomas from MR images using machine intelligence. J Digit Imaging 2017; 30(4):469–476.
101. Aghi M, Gaviani P, Henson JW, et al. Magnetic resonance imaging characteristics predict epidermal growth factor receptor amplification status in glioblastoma. Clin Cancer Res. 2005; 11(24):8600–8605.
102. Rathore S, Akbari H, Rozycki M, et al. Radiomic MRI signature reveals three distinct subtypes of glioblastoma with different clinical and molecular characteristics, offering prognostic value beyond IDH1. Sci Rep 2018; 8(1):1–12.
103. Li Y, Liu X, Xu K, et al. MRI features can predict EGFR expression in lower grade gliomas: a voxel-based radiomic analysis. Eur Radiol. 2018; 28(1):356–362.
104. Kickingereder P, Bonekamp D, Nowosielski M, et al. Radiogenomics of glioblastoma: machine learning–based classification of molecular characteristics by using multiparametric and multiregional MR imaging features. Radiology 2016; 281(3):907–918.

105. Akbari H, Bakas S, Pisapia JM, et al. In vivo evaluation of EGFRvIII mutation in primary glioblastoma patients via complex multiparametric MRI signature. Neuro Oncol 2018; 20(8):1068–1079.
106. Hajianfar, G., I. Shiri, H. Maleki, et al., Non-Invasive MGMT Status Prediction in GBM Cancer Using Magnetic Resonance Images (MRI) Radiomics Features: Univariate and Multivariate Machine Learning Radiogenomics Analysis. arXiv preprint arXiv:1907.03495, 2019.
107. Li Z-C, Bai H, Sun Q, et al. Multiregional radiomics features from multiparametric MRI for prediction of MGMT methylation status in glioblastoma multiforme: a multicentre study. Eur Radiol 2018; 28(9):3640–3650.
108. Korfiatis P, Erickson B. Deep learning can see the unseeable: predicting molecular markers from MRI of brain gliomas. Clin Radiol 2019.
109. Rathore S, Akbari H, Bakas S, et al. Multivariate Analysis of Preoperative Magnetic Resonance Imaging Reveals Transcriptomic Classification of de novo Glioblastoma Patients. Front Comput Neurosci. 2019; 13.
110. Macyszyn L, Akbari H, Pisapia JM, et al. Imaging patterns predict patient survival and molecular subtype in glioblastoma via machine learning techniques. Neuro Oncol 2015; 18(3):417–425.
111. Labussière M, Boisselier B, Mokhtari K, et al. Combined analysis of *TERT*, *EGFR*, and *IDH* status defines distinct prognostic glioblastoma classes. Neurology 2014; 83(13):1200–1206.
112. Arita H, Kinoshita M, Kawaguchi A, et al. Lesion location implemented magnetic resonance imaging radiomics for predicting IDH and TERT promoter mutations in grade II/III gliomas. Sci Rep 2018; 8(1):1–10.
113. Fukuma R, Yanagisawa T, Kinoshita M, et al. Prediction of IDH and TERT promoter mutations in low-grade glioma from magnetic resonance images using a convolutional neural network. Sci Rep 2019; 9 (1):20311.
114. Chen R, Ravindra VM, Cohen AL, et al. Molecular features assisting in diagnosis, surgery, and treatment decision making in low-grade gliomas. Neurosurg Focus. 2015; 38(3):E2.
115. Zhang Z, Chan AK, Ding X, et al. Glioma groups classified by IDH and TERT promoter mutations remain stable among primary and recurrent gliomas. Neuro Oncol 2017; 19(7):1008–1010.
116. Li Y, Liu X, Qian Z, et al. Genotype prediction of ATRX mutation in lower-grade gliomas using an MRI radiomics signature. Eur Radiol. 2018; 28(7):2960–2968.
117. Pan C-c, Liu J, Tang J, et al. A machine learning-based prediction model of H3K27M mutations in brainstem gliomas using conventional MRI and clinical features. Radiother Oncol. 2019; 130:172–179.
118. Park YW, Han K, Ahn SS, et al. Prediction of IDH1-Mutation and 1p/19q-Codeletion Status Using Preoperative MR Imaging Phenotypes in Lower Grade Gliomas. AJNR Am J Neuroradiol 2018; 39(1):37–42.
119. Tian Q, Yan LF, Zhang X, et al. Radiomics strategy for glioma grading using texture features from multiparametric MRI. J Magn Reson Imaging 2018; 48(6):1518–1528.
120. De Looze C, Beausang A, Cryan J, et al. Machine learning: a useful radiological adjunct in determination of a newly diagnosed glioma's grade and IDH status. J. Neurooncol. 2018; 139(2):491–499.
121. Gao Y, Shi Z, Wang Y, et al. Histological grade and type classification of glioma using Magnetic Resonance Imaging. In: 2016 9th International Congress on Image and Signal Processing, BioMedical Engineering and Informatics (CISP-BMEI); 2016.
122. Ranjith G, Parvathy R, Vikas V, et al. Machine learning methods for the classification of gliomas: Initial results using features extracted from MR spectroscopy. Neuroradiol J 2015; 28(2):106–111.
123. Paech D, Windschuh J, Oberhollenzer J, et al. Assessing the predictability of IDH mutation and MGMT methylation status in glioma patients using relaxation-compensated multipool CEST MRI at 7.0 T. Neuro Oncol 2018; 20(12):1661–1671.
124. Wiestler B, Kluge A, Lukas M, et al. Multiparametric MRI-based differentiation of WHO grade II/III glioma and WHO grade IV glioblastoma. Sci Rep 2016; 6(1):1–6.
125. Wang X, Wang D, Yao Z, et al. Machine learning models for multiparametric glioma grading with quantitative result interpretations. Front Neurosci. 2019; 12:1046.
126. Lo C-M, Chen Y-C, Weng R-C, et al. Intelligent Glioma Grading Based on Deep Transfer Learning of MRI Radiomic Features. Appl. Sci. 2019; 9:4926.
127. Yang Y, Yan LF, Zhang X, et al. Glioma Grading on Conventional MR Images: A Deep Learning Study With Transfer Learning. Front Neurosci 2018; 12:804.
128. Osman AFI. Automated Brain Tumor Segmentation on Magnetic Resonance Images and Patient's Overall Survival Prediction Using Support Vector Machines. Cham: Springer International Publishing, 2018.
129. Bae S, Choi YS, Ahn SS, et al. Radiomic MRI Phenotyping of Glioblastoma: Improving Survival Prediction. Radiology 2018; 289(3):797–806.
130. Jones PS, Carroll KT, Koch M, et al. Isocitrate Dehydrogenase Mutations in Low-Grade Gliomas Correlate With Prolonged Overall Survival in Older Patients. Neurosurgery 2019; 84(2):519–528.
131. Suchorska B, Schuller U, Biczok A, et al. Contrast enhancement is a prognostic factor in IDH1/2 mutant, but not in wild-type WHO grade II/III glioma as confirmed by machine learning. Eur J Cancer 2019; 107:15–27.
132. Yang D, Rao G, Martinez J, et al. Evaluation of tumor-derived MRI-texture features for discrimination of molecular subtypes and prediction of 12-month survival status in glioblastoma. Med Phys 2015; 42(11):6725–6735.
133. Sun L, Zhang S, Chen H, et al. Brain Tumor Segmentation and Survival Prediction Using Multimodal MRI Scans With Deep Learning. Frontiers in Neurosci 2019; 13(810).
134. Sanghani P, Ang BT, King NKK, et al. Overall survival prediction in glioblastoma multiforme patients from volumetric, shape and texture features using machine learning. Surg Oncol. 2018; 27(4):709–714.
135. Chaddad A, Sabri S, Niazi T, et al. Prediction of survival with multi-scale radiomic analysis in glioblastoma patients. Med Biol Eng Comput 2018; 56(12):2287–2300.
136. Lee MH, Kim J, Kim ST, et al. Prediction of IDH1 Mutation Status in Glioblastoma Using Machine Learning Technique Based on Quantitative Radiomic Data. World Neurosurg 2019; 125:e688–e696.
137. Gevaert O, Mitchell LA, Achrol AS, et al. Glioblastoma Multiforme: Exploratory Radiogenomic Analysis by Using Quantitative Image Features. Radiology 2014; 273(1):168–174.
138. Rios Velazquez E, Meier R, Dunn Jr WD, et al. Fully automatic GBM segmentation in the TCGA-GBM dataset: Prognosis and correlation with VASARI features. Sci Rep 2015; 5(1):16822.
139. Gutman DA, Dunn WD, Grossmann P, et al. Somatic mutations associated with MRI-derived volumetric features in glioblastoma. Neuroradiology 2015; 57(12):1227–1237.
140. Peeken JC, Hesse J, Haller B, et al. Semantic imaging features predict disease progression and survival in glioblastoma multiforme patients. Strahlenther Onkol. 2018; 194(6):580–590.
141. Chato L, Latifi S. Machine Learning and Deep Learning Techniques to Predict Overall Survival of Brain Tumor Patients using MRI Images. In: 2017 IEEE 17th International Conference on Bioinformatics and Bioengineering (BIBE); 2017.
142. Li Q, Bai H, Chen Y, et al. A Fully-Automatic Multiparametric Radiomics Model: Towards Reproducible and Prognostic Imaging Signature for Prediction of Overall Survival in Glioblastoma Multiforme. Sci Rep 2017; 7(1):14331.
143. Shboul ZA, Vidyaratne L, Alam M, et al. Glioblastoma and Survival Prediction. Cham: Springer International Publishing, 2018.
144. Han W, Qin L, Bay C, et al. Deep Transfer Learning and Radiomics Feature Prediction of Survival of Patients with High-Grade Gliomas. AJNR Am J Neuroradiol 2020; 41(1):40–48.
145. Nie D, Lu J, Zhang H, et al. Multi-Channel 3D Deep Feature Learning for Survival Time Prediction of Brain Tumor Patients Using Multi-Modal Neuroimages. Sci Rep 2019; 9(1):1103.
146. Lao J, Chen Y, Li Z-C, et al. A Deep Learning-Based Radiomics Model for Prediction of Survival in Glioblastoma Multiforme. Sci Rep 2017; 7 (1):10353.
147. Clark K, Vendt B, Smith K, et al. The Cancer Imaging Archive (TCIA): maintaining and operating a public information repository. J Digit Imaging 2013; 26(6):1045–1057.
148. Bakas S, Akbari H, Sotiras A, et al. Advancing the cancer genome atlas glioma MRI collections with expert segmentation labels and radiomic features. Sci data 2017; 4:170117.
149. Schlett CL, Hendel T, Hirsch J, et al. Quantitative, organ-specific interscanner and intrascanner variability for 3 T whole-body magnetic resonance imaging in a multicenter, multivendor study. Invest Radiol. 2016; 51(4):255–265.

150. Fortin J-P, Cullen N, Sheline YI, et al. Harmonization of cortical thickness measurements across scanners and sites. Neuroimage 2018; 167:104–120.
151. Yu M, Linn KA, Cook PA, et al. Statistical harmonization corrects site effects in functional connectivity measurements from multi-site fMRI data. Hum Brain Mapp. 2018; 39(11):4213–4227.
152. Meng Y, Sun J, Qu N, et al. Application of Radiomics for Personalized Treatment of Cancer Patients. Cancer Manag Res. 2019; 11:10851–10858.
153. Liu Z, Wang S, Dong D, et al. The Applications of Radiomics in Precision Diagnosis and Treatment of Oncology: Opportunities and Challenges. Theranostics 2019; 9(5):1303–1322.
154. Banerjee S, Mitra S, Shankar BU, et al. A Novel GBM Saliency Detection Model Using Multi-Channel MRI. PloS one 2016; 11(1):e0146388.
155. Sheller MJ, Reina GA, Edwards B, et al. Multi-institutional deep learning modeling without sharing patient data: A feasibility study on brain tumor segmentation. International MICCAI Brainlesion Workshop. Springer, 2018.